Development of Photochemical Systems Based on Photoinduced Electron Transfer

榎本　孝文

博士（理学）

総合研究大学院大学
物理科学研究科
構造分子科学専攻

平成３０（２０１８）年度

Development of Photochemical Systems Based on Photoinduced Electron Transfer

光誘起電子移動に立脚した光化学反応系の開発

Takafumi Enomoto

March 2019

Department of Structural Molecular Science
School of Physical Sciences
SOKENDAI (The Graduate University for Advanced Studies)

Preface

The study presented in this thesis has been carried out under the direction of Dr. Shigeyuki Masaoka during April 2014 – March 2019 at the Department of Structural Molecular Science, School of Physical Science, SOKENDAI (The Graduate University for Advanced Studies).

The author is greatly indebted to Dr. Shigeyuki Masaoka for his significant guidance, continuous encouragement, and valuable discussion. The author also wishes to express her sincere gratitude to Dr. Mio Kondo for her kind suggestion, hearty encouragement, and helpful discussion.

The author is deeply grateful to Dr. Neal Devaraj, Dr. Roberto Brea, Mr. Ahanjit Bhattacharya, and all lab members in Devaraj group (University of California, San Diego) for their kind discussion and fruitful suggestion. The author also grateful to Dr. Lee Sze Koon (Institute for Molecular Science) and Ms. Daphne Cheung Po Ling (University of California, San Diego) for their great support during his stay in San Diego.

The author wishes to express his appreciation to Dr. Norio Narita (The University of Tokyo) and Dr. Nobuhiko Kusakabe (National Astronomical Observatory of Japan) for giving him a great opportunity to join the project in astrobiology. The author thankful to Dr. Motomu Kanai, Dr. Kounosuke Oisaki, Mr. Takayuki Wakaki, and Mr. Kentaro Sakai (The University of Tokyo) for valuable discussion for hybrid catalysis.

The author expresses his gratitude to Dr. Toshikazu Nakamura and Dr. Mizue Asada (Institute for Molecular Science) for the measurement of ESR spectroscopy. The author is thankful to Mr. Seiji Makita (Institute for Molecular Science) for the measurement of elemental analysis. The author is grateful to Ms. Michiko Nakano and Ms. Haruyo Nagao (Institute for Molecular Science) for the measurement of NMR spectroscopy.

The author is grateful to Dr. Norie Momiyama, Dr. Atsuto Izumiseki, Dr. Takuya Kurahashi (Institute for Molecular Science), Dr. Hidehiro Sakurai (Osaka University), Dr. Shuhei Higashibayashi (Keio University), Dr. Koji Yamamoto (Gunma University), Dr. Koji Yamamoto (Tokyo Institute of Technology), and all members in the joint seminar in Yamate Campus of Institute for Molecular Science for their fruitful discussion.

The author expresses his sincere appreciation to current members and alumni of Masaoka group, Dr. Masaya Okamura, Dr. Vijayendran K. K. Praneeth, Dr. Pondchanok Chinapang, Mr. Hitoshi Izu, Mr. Hikaru Iwami, Ms. Mami Kachi, Mr. Masahiro Tasaki, Mr. Takuya Akai, Ms. Mei Ishihara, Mr. Soshi Kato, Ms. Misa Tomoda, Ms. Mayu Fujisawa, Dr. Go Nakamura, Dr. Takahiro Itoh, Dr. Yuki Okabe, Dr. Arisa Fukatsu, Dr. Lee Sze Koon, Mr. Ke Liu, Ms. Yukino Fukahori, Mr. Riku Ushijima, and Ms. Chihiro Matsui for their precious friendship and invaluable discussion. The author appreciates the kind support from technical staffs, Ms. Miho Matsuda, Ms. Mari Kanaike, Ms. Reiko Kuga, and Ms. Akane Shibata. The author is deeply grateful to Ms. Mayuko Taniwake and Ms. Kyoko Nogawa for their administration work. The author wishes to thank friendship and fruitful discussions from all of short-term visitors in Masaoka Group.

The author expresses his gratitude to Mr. Mitsuki Yamashita, Mr. Masahiro Teramoto, Mr. Kiyohiro Adachi, Dr. Naoya Ohtsuka, Mr. Shosei Kubo, Mr. Kohei Tsukada, Mr. Naoki Shinoda, Mr. Atsushi Asami, Mr. Takanari Azami, Mr. Hiroki Okawa, Mr. Tomohiro Kanda, Mr. Yusuke Sakuragi, Mr. Yuki Terashima, and Mr. Katsushi Oshima for their precious friendship and invaluable encouragement.

The author is much indebted for the financial support of Research Fellowships of the Japan Society for the Promotion of Science for Young Scientists, IMS SRA support, and Course-by-Course Education Program to Cultivate Researchers in Physical Sciences with Broad Perspectives of SOKENDAI.

Finally, the author wishes to offer special thanks to his parents Mr. Nobuhide Enomoto and Ms. Naoko Enomoto, his grand-mother Ms. Mitsuyo Enomoto for their all patience, constant financial support, and warmhearted encouragement.

Takafumi Enomoto

Okazaki

March, 2019

Contents

General Introduction

Overview of Photoinduced Electron Transfer

Photoinduced electron transfer (PET) is at the heart of many schemes in both natural and artificial chemical systems because PET is a crucial chemical process involving a conversion of light stimuli to electrochemical events. PET reaction is initiated by the absorption of a photon by a dye molecule (Dye) as shown in Scheme 1-(1). When a photon collides to Dye, Dye absorbs the photon if the energy of the photon matches with the energy difference between the ground state and the electronic excited state of Dye, and the excited species of Dye (Dye*) generates. Dye* normally relaxes to the ground state through a variety of deactivation pathways, such as vibrational relaxation, internal conversion and photoluminescence (Scheme 1-(2)). However, when Dye* collides to a substrate (X) before relaxing to the ground state, a chemical reaction between Dye* and X can proceed. PET is defined as a photochemical process which involves an electron transfer reaction between Dye* and X (Scheme 1-(3)). Generally, a photochemically excited molecule has stronger oxidation/reduction power than its ground state species, and thus the electron transfer reactions which cannot proceed with the ground state species can occur in PET reactions. By utilizing such feature of PET, numerous reports on the development of photoenergy conversion systems[1-3] and photochemical molecular transformations[4-6] have been conducted. Moreover, PET is also widely used as a powerful tool for the spatiotemporal control of chemical reactions because the PET reaction proceeds only in the space irradiated by light[7-9].

In PET reactions, the reactivity of Dye* for the electron transfer reaction is of vital importance. There are two essential factors determining the reactivity of Dye*; the lifetime and the redox potential of Dye*. In order to complete the electron transfer reaction between Dye* and X, the lifetime of Dye* must be comparable to the timescale of the intermolecular electron transfer reaction. Furthermore, the redox potentials of Dye* should be estimated precisely to select an appropriate substrate for the electron transfer reaction. From the next section, the details of these essential factors for the construction of PET systems are described.

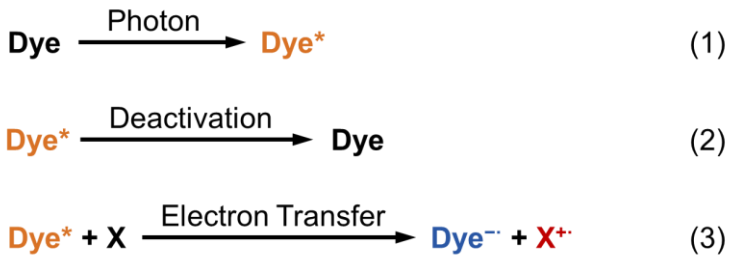

Scheme 1. Reaction schemes related to PET reaction.

Excitation Lifetime

As described above, PET requires an electron transfer reaction between Dye* and X. In homogeneous solution, an electron transfer reaction between independent Dye* and X proceeds via diffusion process. Therefore, the excitation lifetime of Dye* should be comparable to the collision frequency between Dye* and X. The lifetime of Dye* is determined by the rates of the nonradiative deactivation pathways except for the case where the luminescence quantum yield of Dye* is close to 1. The nonradiative deactivation pathways are classified into two categories; internal conversion and intersystem crossing.

Internal conversion is an electronic transition from a lowest singlet excited state (S_1) with a vibrationally ground state ($v' = 0$) to a singlet ground state (S_0) with a vibrationally excited state ($v > 0$). The rate of the internal conversion is related to the overlapping integral of nuclear coordinates between before and after the internal conversion, which is called as Franck-Condon factor, as given in equation (4).

$$\int (x_N)_f \quad (x_N)_i \ \mathrm{dt} \qquad (4)$$

$(x_N)_f$ is the nuclear coordinate of Dye after internal conversion, and $(x_N)_i$ is the nuclear coordinate of Dye before internal conversion. The value of the Franck-Condon factor becomes smaller as the difference of the nuclear coordinates between before and after internal conversion becomes larger. The differences between these nuclear coordinates are dependent on the difference of energies between S_0 and S_1 (ΔE_S), and the rate constant of the internal conversion (k_{IC}) is given by equation (5) with molecular parameter β.

$$k_{IC} \propto \exp(-\beta \Delta E_s) \qquad (5)$$

This equation clearly indicates that the rate of the internal conversion is dramatically accelerated by decreasing the value of ΔE_S. This relationship is known as Energy Gap Rule of internal conversion[10].

Intersystem crossing is an electronic transition which accompanies the inversion

of electronic spins. In order to promote the transition with the spin inversion, the rate constant of the intersystem crossing is affected by not only the Franck-Condon factor but also electronic spin-orbit interaction, which leads the mixing of several electronic configurations with different spin multiplicities. Although the transition between the electronic states with different spin multiplicities is forbidden, the intersystem crossing can proceed due to the spin-orbit interaction. For instance, in the case of carbonyl compounds, the mixing of the electronic configurations of the singlet n-π* excited state with the triplet π-π* excited state occurs, and the probability of the intersystem crossing from singlet n-π* state to triplet π-π* state becomes non-zero. Generally, a rate of an electronic transition from a triplet excited state to a singlet ground state is much slower than that from a singlet excited state to a singlet ground state. Therefore, the large transition probability of the intersystem crossing leads to the efficient generation of the long lifetime triplet excited state.

Redox Potentials of Excited Species

The electron transfer reactions of the excited molecules can be dealt with in the theory of electron transfer process of ground state molecules, and the changes of the free energy of the electron transfer reaction can be calculated from the redox potentials of molecules involving the reaction. Therefore, the estimation of the redox potentials of the excited dye molecule (Dye*) is highly important for the construction of novel PET systems. The methods described here are two common ways to estimate the redox potentials of Dye*.

One of the most common methods for estimating the redox potentials of the excited species is making Rehm-Weller plot[11]. In this method, quenching experiments of Dye* with several substrates (X) with known redox potentials are conducted, and a variety of bimolecular quenching rate constants (k_q) are determined. When the natural logarithms of k_q values ($\ln k_q$) are plotted versus corresponding redox potentials of X, the plot shows a linear relationship when the reduction/oxidation power of X is relatively weak, and then the $\ln k_q$ value reaches the diffusion limit as the reduction/oxidation power of X becomes stronger. The value of the redox potential at the inflection point of the plot can be regarded as the redox potential of Dye* (Figure 1).

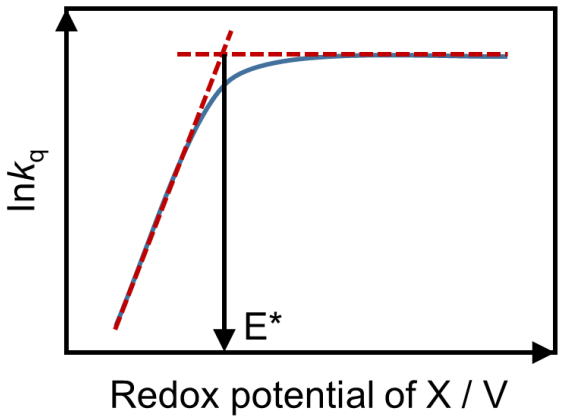

Figure 1. An illustrated example of Rehm-Weller plot.

In order to determine the quenching rate constants (k_q), Stern-Volmer plot is widely used. When the Dye* is emissive, Stern-Volmer equation is written as follows:

$$\frac{I_0}{I} = k_{obs}\ [X] + 1, \qquad k_{obs} = k_q \tau_l \qquad (6)$$

where, I_0 is a luminescence intensity of Dye in the absence of X, I is a luminescence intensity of Dye in the presence of X, k_{obs} is an apparent quenching rate constant and [X] is the concentration of X. The plot [X] versus I_0/I gives the value of k_{obs} as the slope. k_{obs} is expressed by the multiply of k_q and the luminescence lifetime of Dye (τ_l). Therefore, the value of k_q can be determined by using τ_l value, which can be determined by the luminescence lifetime measurement. When the electron transfer reaction between Dye* and X proceeds through the collision between Dye* and X, the Stern-Volmer equation can be expressed with the excitation lifetimes of Dye* (eq. 7):

$$\frac{\tau_0}{\tau} = k_{obs}\ [X] + 1, \qquad k_{obs} = k_q \tau_0 \qquad (7)$$

where, τ_0 is an excitation lifetime of Dye in the absence of X, and τ is an excitation lifetime of Dye in the presence of X. The Stern-Volmer plots also can be used for mechanistic studies as described in the next section.

The redox potentials of the excited species also can be estimated using the redox potentials of the ground state species and its excitation energy. For estimating the oxidation potential of Dye* (E_{ox}*), a zero-zero transition energy of Dye (E_{00}) is subtracted from the oxidation potential of Dye (E_{ox}) determined by electrochemical techniques (eq. 8):

$$E_{ox}^* = E_{ox} - E_{00} \qquad (8)$$

On the other hand, the reduction potential of Dye* (E_{red}*) can be estimated by the addition of E_{00} to the oxidation potential of Dye (E_{red}, eq. 9):

$$E_{red}^* = E_{red} + E_{00} \qquad (9)$$

The value of E_{00} can be estimated by the steady state luminescence measurements. Note that, the value of E_{00} must be determined by the phosphorescence spectrum of Dye at low temperature (e.g. 77 K) when the PET reaction proceeds between the triplet excited species and the substrate. It should be also noted that this method is not necessary to afford the same result of Rehm-Weller plot because this method is rough estimations.

Quenching Mechanisms

Mechanistic studies are highly important for understanding the reaction mechanisms of PET. PET systems, which composed of a dye molecule (Dye) and a substrate (X), are classified into two categories according to the role of X[12]. When the X works as an oxidant, an electron from Dye* is transferred to the vacant orbital of X (Figure 2a). This quenching process is called as an oxidative quenching. On the other hand, a reductive quenching proceeds via electron transfer from X to Dye* (Figure 2b).

PET systems are also classified into two categories according to the quenching dynamics: dynamic and static quenching systems[13] (Figure 3). When the ground state species of Dye and X do not interact with each other, the PET reaction proceeds via collision of Dye* and X. This quenching mechanism is called as a dynamic quenching. The system is suitable for systematic investigations of PET with various combinations of Dye and X by simply mixing these components, although the relatively long excitation lifetime of Dye is required to realize the intermolecular electron transfer process. On the other hand, if the ground state species of Dye and X interact with each other, the electron transfer reaction between Dye* and X does not require the collision of Dye* and X. This quenching mechanism is called as a static quenching. In the static quenching, the electron transfer between Dye* and X proceeds within short timescale (-ps)[14], and thus, a dye molecule with a short lifetime can be utilized. However, the construction of the system usually requires complicated synthetic procedures because the formation the assembled structure of Dye and X is necessary. The quenching mechanisms of PET systems can be judged from the slope of a Stern-Volmer plot based on the excitation lifetime (Figure 3). If the slope of Stern-Volmer plot is not zero, the PET reaction proceeds via dynamic quenching mechanism, and if the slope is zero, the PET reaction proceeds via static quenching mechanism.

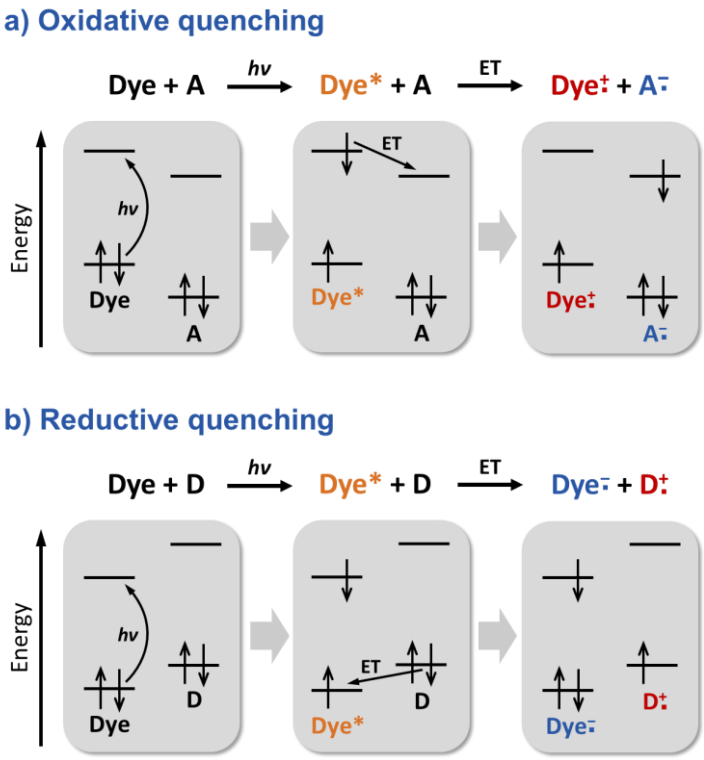

Figure 2. Schematic representation of PET reactions via reductive / oxidative quenching.

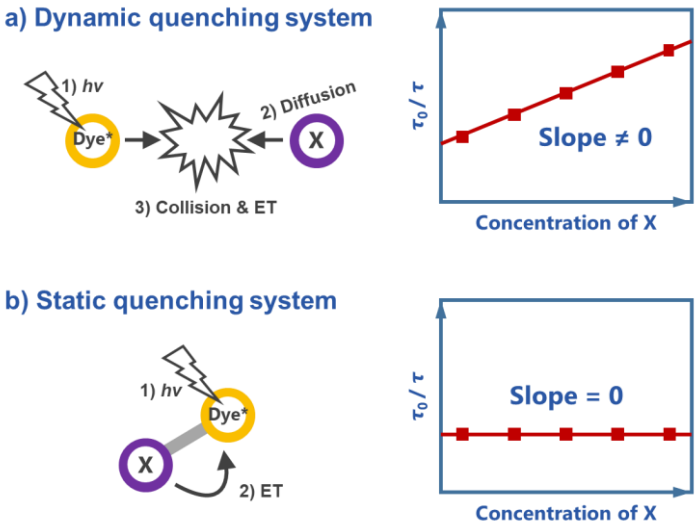

Figure 3. Schematic illustration of PET reactions which proceed via a) dynamic and b) static quenching (Left). Illustrated examples of Stern-Volmer plots of PET reactions which proceed via a) dynamic and b) static quenching (Right) .

Photoinduced Electron Transfer Driven by Near-Infrared Light

The utilization of near-infrared (NIR) light (> 700 nm), which covers more than 40% energy in sun light reaching on the earth, is a highly important objective for the use of solar energy with high efficiency[15,16]. In this context, extensive efforts have been made for developing materials with NIR absorption so far[17,18]. The most common way to tune the absorption band of dye molecules to the longer wavelength region is the extension of π-system of the dye (Figure 4, left).[19,20] By extending the conjugation length of the π system, the HOMO-LUMO gap of the dye becomes smaller and the absorption band shifts to the longer wavelength region. Another approach is the use of donor-acceptor connected chromophores (Figure 4, center).[21,22] The hybridization of the orbitals of the donor and the acceptor moieties results in the absorption band in the longer wavelength region. Open-shell radicals are also utilized as NIR absorbing material because SOMO-LUMO or HOMO-SOMO gaps are normally smaller than HOMO-LUMO gap (Figure 4, right).[23]

In order to construct PET systems bearing NIR absorbing chromophores, molecular dyads comprising NIR absorbing dyes and electron donor/accepter moieties are currently investigated[24-74] (Table 1). However, most of these studies have demonstrated the PET reactions driven by visible light (≤ 700 nm), and there are only a few reports on NIR light-induced electron transfer (NIR-ET) systems. Furthermore, all the reports on NIR-ET systems are limited to static quenching systems.

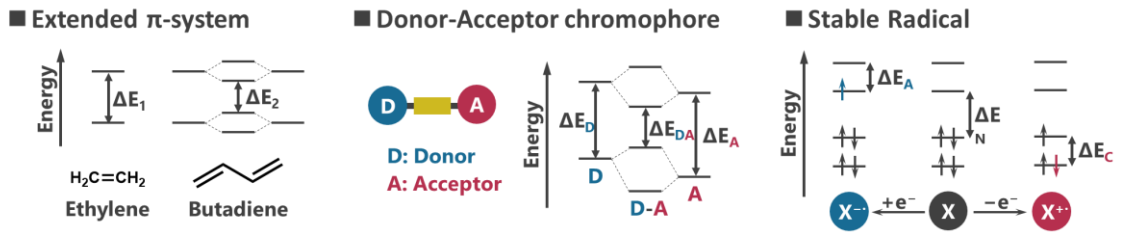

Figure 4. Schematic illustration of strategies for tuning the absorption band of dye molecule to the longer wavelength region.

Table 1. Summary of PET systems using NIR light absorbing compounds in homogeneous media. In most of the existing PET systems, the photochemical reactions were initiated by the irradiation of the visible light (≤ 700 nm), and there are only several reports on the PET systems which employ NIR light as light source (> 700 nm). Moreover, there have been no reports on a NIR-ET system based on dynamic quenching mechanism. Note that reports on NIR-ET systems in heterogeneous media, such as dye sensitized solar cell, were not included in the table because PET reactions in these systems proceed via static quenching mechanism.

System	Excitation	Absorption maxima	Quenching Mechanism	Reference
$C_{60}^{-\bullet}$-A (A = PhDI, NDI, $NDI^{-\bullet}$, $PDI^{-\bullet}$)	1000, 715, 765 nm	765-1003 nm	Static	24
$PDI^{-\bullet}$-Re	950 nm	ca. 955 nm	Static	25
Fc-BDP-Mer	800 nm	810 - 818 nm	Static	26
$[Ru_3(dmbpy)_6(\mu\text{-HAT})]^{6+}$-$Asc^-$	700 – 800 nm	600 nm	Static	27
$PDI^{-\bullet}$-A (A = PhI, NI, PhDI, NDI, PDI,$PDI^{-\bullet}$)	700 nm	ca. 955 nm	Static	28
ZnPc-PDI	685 nm	681 nm	Static	29
ZnPc + BQ	680 nm	ca. 700 nm	Dynamic	30
D-BDP-Crown-C_{60} (D = NPh_3, PTZ, Fc, Ph)	654 nm	654-658 nm	Static	31
ZnPc-PDI	640 nm	690-707 nm	Static	32
PDI-$(RuCOPc)_4$	630 nm	719 nm	Static	33
azaBDP-Fc_2	630 nm	706 nm	Static	34
PBDP-Fc_2	620 nm	651 nm	Static	35
BDP-Fc_n (n = 1, 2)	619 nm	671-750 nm	Static	36
$Rh_2(DTolF)_2(npCOO)_2$ + MV	> 610 nm	640 nm	Dynamic	37
$NDI^{-\bullet}$-PMI	605 nm	ca. 760 nm	Static	38
TPA-BDP-A (A = C_{60}, H)	600 nm	691 nm	Static	39
$Re_2bpyNNH_2bpy$-$H_3PW_{12}O_{40}$	580-680 nm	725 nm	Static	40
BDP-SiPc-MSBDP	550 nm	682 nm	Static	41
$NDI^{-\bullet}$-NI	532 nm	ca. 760 nm	Static	38
SiPc-BDP_2	480, 530 nm	683 nm	Static	42
ZnPc-PDI	530 nm	681 nm	Static	43
PDI-A (A = C_{60}, $C_{59}N$)	510 nm	632-638 nm	Static	44
UCyFPP + **$AcrH_2$**	490 nm	1177 nm	Dynamic	45
Fc-azaBDP-C_{60}	480 nm	ca. 635 nm	Static	46
$NDI^{-\bullet}$-A (A = PDI, PI)	475 nm	ca. 760 nm	Static	38
PTZ_2-azaBDP-C_{60}	460 nm	643 nm	Static	47
azaBDP-Fc_n (n = 1, 2)	440 nm	655-700 nm	Static	48
ZnPc + $ZnPcH^+$	430 nm	836 nm	Dynamic	49

Table 1. (Continued)

System	Excitation	Absorption maxima	Quenching Mechanism	Reference
ZnNc-NDI	430 nm	769 nm	Static	50
DPP-(ZnPc)$_n$ (n = 1,2)	430 nm	680-705 nm	Static	51
MPc-C$_{60}$ (M = Zn, H$_2$)	420 nm	700-737 nm	Static	52
PDI-C$_{60}$	420 nm	718 nm	Static	53
PDI-SiPc-C$_{60}$	420 nm	695 nm	Static	54
C$_{60}$-ZnPc-ZnPor-C$_{60}$	430 nm	682 nm	Static	55
BDP-Por$_2$	420 nm	665 nm	Static	56
PDI-C$_{60}$	415 nm	700 nm	Static	57
PDI-(ZnPc)$_n$ (n = 1,2)	410 nm	ca. 681 nm	Static	58
BABDP-C$_{60}$	400 nm	828 nm	Static	59
D-BDP-C$_{60}$ (D =TPA, PTZ)	400 nm	676-702 nm	Static	60
azaBDP-(SubPc)$_2$	400 nm	695 nm	Static	61
D-BDP-Crown-C$_{60}$ (D = TPA, PTZ)	400 nm	686-697 nm	Static	62
PEG$_4$ZnPc-ImC$_{60}$	400 nm	683 nm	Static	63
SubPc-azaBDP-C$_{60}$	400 nm	678 nm	Static	64
BDP-azaBDP-A (A = C$_{60}$, H)	400 nm	663-667 nm	Static	65
SubPc-C$_{60}$	400 nm	649-653 nm	Static	66
ZnNc-PDI	390 nm	769 nm	Static	67
azaBDP-D$_2$ (D = ZnPc, ZnNc)	390 nm	691-768 nm	Static	68
D$_2$-azaBDP-C$_{60}$ (D = DMAP, TP, Fc, H)	390 nm	640-720 nm	Static	69
Fc-BDP-A (A = C$_{60}$, H)	390 nm	ca. 700 nm	Static	70
D-azaBDP-A (D = BDP, H; A = C$_{60}$, H)	390 nm	697-700 nm	Static	71
ZnPc-AuPpy	390 nm	681 nm	Static	72
PDI-(ZnPc)$_2$	387 nm	710 nm	Static	73
SiPc-(C$_{59}$N)$_n$ (n = 1,2)	355 nm	692-693 nm	Static	74

BIH = 1,3-dimethyl-2-phenyl- benzimidazoline, C_{60} = fullerene, PhDI = phthaldiimide, NDI = naphthaldiimide, PDI = perylene diimide, Re = Re(bpy)$(CO)_3$(py), Fc = ferrocene, BDP = boron dipyrromethane, Mer = merocyanine, dmbpy = 4,4'-dimethyl-2,2'-bipyridine, HAT = 1,4,5,8,9,12-hexaazatriphenylene, Asc = ascorbate, Pc = phthalocyanine, PhI = phthalimide, NI = naphthalimide, BQ = benzoquinone, Crown = crown ether, PTZ = phenothiazine, azaBDP = boron azadipyrromethane, PBDP = pyridine-BDP, DTolF = *p*-ditolylformamidinate, npCOO = 1,8-naphthyridine-2-

carboxylate, MV = methyl viologen, PMI = perylene imide, TPA = triphenylamine, bpy = 4,4'-bipyridine, MS = monostylene, $C_{59}N$ = azafullerene, UCyFPP = uranyl cyclo[1]furan[1]pyridine[4]pyrrole, $AcrH_2$ = dihydromethylacridine, $AcrH_2$ = 9,10-dihydro-10-methylacridine Nc = naphthalocyanine, DPP = diketopyrrolopyrrole, Por = porphyrin, BABDP = benzannulated boron azadipyrromethane, subPc = subphthalocyanine, PEG = polyethylene glycol, DMAP = dimethylaminophenyl, Ppy = tetrapyridylporphyrin,.

Photoinduced Proton Coupled Electron Transfer

In natural photosynthetic systems, an efficient proton transport is achieved by using PET reaction coupled with proton transfer reaction to realize the effective chemical energy production[75,76]. Inspired by the natural system, studies on the construction of artificial PET systems conjugated with proton transfer have attracted attention[77-79]. Electron transfer reactions conjugated with proton transfer is well known as proton coupled electron transfer (PCET) reaction, and it is at the heart of many schemes in both chemistry and biology. The PCET is classified into 4 categories based on the mechanisms[80-82]; sequential proton transfer-electron transfer (PT-ET), sequential electron transfer-proton transfer (ET-PT), concerted proton-electron transfer (CPET) and hydrogen atom transfer (HAT) (Figure 5). PT-ET or ET-PE processes proceed stepwise mechanism of electron and proton transfer via the formation of intermediate states. On the other hand, when an electron and a proton are transferred at the same time and no intermediate states are observed, such PCET processes are classified as CPET or HAT. The difference between CPET and HAT is the direction of the electron and the proton transfer[83] (Figure 6). If an electron and a proton are transferred to different orbitals, the process is CPET, and if an electron and a proton are transferred to same orbital, the process is HAT. CPET and HAT are favored with a shallow activation barrier because these processes proceed via single kinetic step circumventing the formation of charged intermediate state.

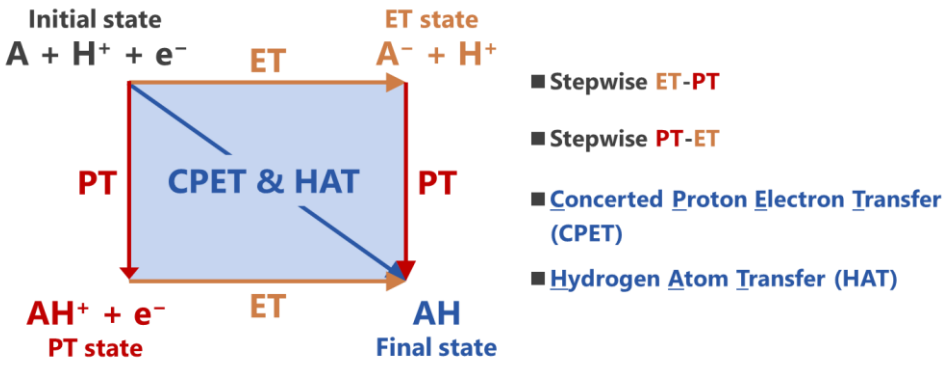

Figure 5. Schematic representation of PCET reactions.

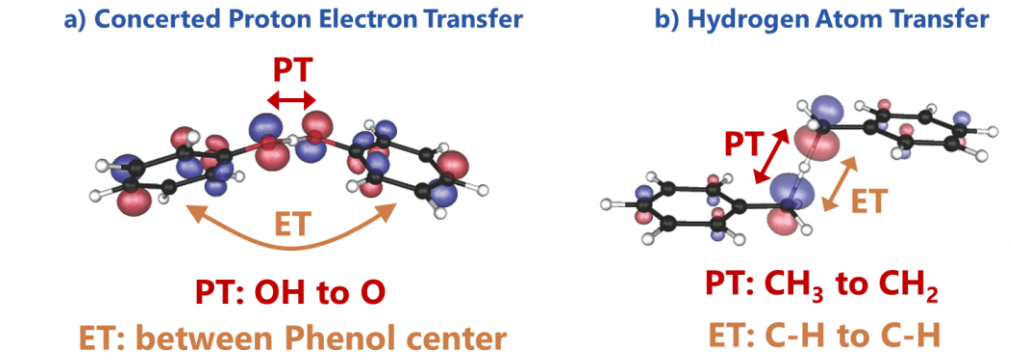

Figure 6. Illustrations of CPET and HAT based on the insight of molecular orbitals.

Spatiotemporal Control of Chemical Reaction using Photoinduced Electron Transfer

Spatial and temporal control of chemical reaction by external stimuli is highly important in not only fundamental importance for understanding chemical reactions but also potential applications for developing functional materials. One of the most common external stimuli for controlling chemical reaction is a photo-stimulus[84,85]. The photo-stimulus has high spatiotemporal controllability and is easy to handle. Because of these reasons, the photo-stimulus are widely used for controlling chemical reactions even in industrial use such as photolithography[86]. Recently, the photochemical control of an artificial phospholipid membrane formation based on the PET reaction is reported[87]. From the view point of synthetic biology, the development of the methodologies for preparing the artificial phospholipid membranes are an important objective. However, using the traditional method for preparing phospholipid membranes, the spatiotemporal control of the membrane formation was not available because the membrane formation starts immediately after dissolving phospholipids. Devaraj *et al* developed new methodology to form artificial phospholipid membranes in-situ using click reaction as a key reaction[88]. The conjugation of the click system and PET reaction led to establish the artificial phospholipid membrane formation system triggered by photochemical stimuli (Figure 7).

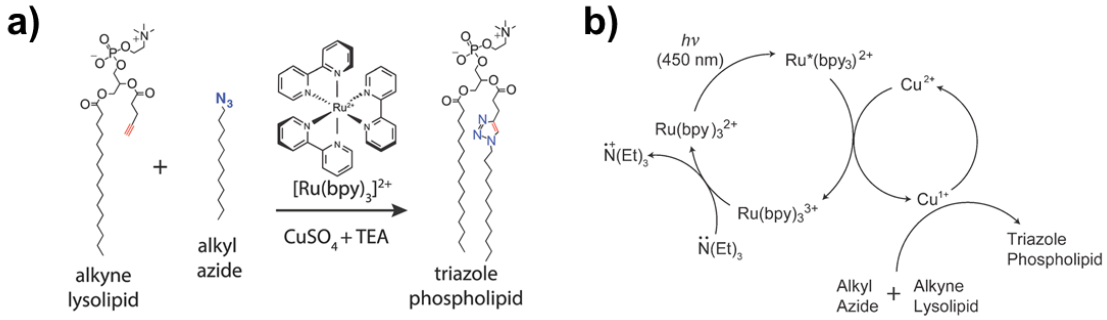

Figure 7. (a) Reaction scheme of the artificial phospholipid membrane formation system. (b) Proposed reaction mechanism of the artificial phospholipid membrane formation reaction triggered by PET reaction.

Aim and Survey of This Thesis

As described above, PET is one of the most essential chemical processes in both fundamental and application use. In this study, the author focused on three points of view for further development of PET; an extension of usable energy of photons in PET reaction to the longer wavelength region than visible light, a conjugation of PET reaction with other chemical reactions, and an application of PET for controlling chemical reaction. For these purposes, the author aimed to develop a NIR-ET system via dynamic quenching mechanism, a NIR-ET system coupled with a proton transfer reaction, and an artificial phospholipid membrane formation system triggered by an intramolecular PET reaction.

Chapter 1 describes a new class of a NIR-ET system using a distorted phthalocyanine as a photosensitizer. The author revealed that the appropriate modification of distorted phthalocyanine affords a near-infrared absorbing dye with high photostability and long excitation lifetime, and a NIR-ET system was successfully established using the dye. The mechanistic investigation clarified that the electron transfer system works via dynamic quenching mechanism. The system generated a long-lived anion radical species of the dye upon near-infrared light irradiation (>750 nm).

Chapter 2 investigates that a phthalocyanine anion which exhibits intense NIR absorption property and electron transfer and proton accepting abilities promoted a PCET reaction induced by NIR light (> 710 nm). The NIR light induced PCET system can generate long-lived radical species by suppressing a back electron transfer reaction and showed high reversibility and robustness.

Chapter 3 describes a new methodology to promote a biomimetic phospholipid membrane formation by a photochemical activation of a catalyst-sensitizer dyad via an intramolecular PET process. First, a CuAAC reaction mediated by a copper-coumarin dyad with water-soluble substrates is demonstrated and it is revealed that the reaction can be initiated by photoirradiation in the absence of any sacrificial reductants. Interestingly, the temporal control of CuAAC reaction is available by on/off switching of photoirradiation. The photocontrolled CuAAC reaction coupled to triazole phospholipid formation leads to a novel methodology for using light to initiate the vesicle formation.

References

(1) Barber, J. *Chem. Soc. Rev.* **2009**, *38*, 185–196.

(2) McConnell, I.; Li, G.; Brudvig, G. W. *Chem. Biol.* **2010**, *17*, 434–447.

(3) Hagfeldt, A.; Boschloo, G.; Sun, L.; Kloo, L.; Pettersson, H. *Chem. Rev.* **2010**, *110*, 6595–6663.

(4) Shaw, M. H.; Twilton, J.; MacMillan, D. W. C. *J. Org. Chem.* **2016**, *81*, 6898–6926.

(5) Romero, N. A.; Nicewicz, D. A. *Chem. Rev.* **2016**, *116*, 10075–10166.

(6) Dadashi-Silab, S.; Doran, S.; Yagci, Y. *Chem. Rev.* **2016**, *116*, 10212–10275.

(7) Michaudel, Q.; Kottisch, V.; Fors, B. P. *Angew. Chem. Int. Ed.* **2017**, *56*, 9670–9679.

(8) Adzima, B. J.; Tao, Y.; Kloxin, C. J.; DeForest, C. A.; Anseth, K. S.; Bowman, C. N. *Nat. Chem.* **2011**, *3*, 256–259.

(9) Ruhl, K. E.; Rovis, T. *J. Am. Chem. Soc.* **2016**, *138*, 15527-15530.

(10) Englman, R.; Jortner, J. *Mol. Phys.* **1970**, *18*, 285–287.

(11) Knibbe, H.; Rehm, D. and Weller, A. Ber. Bunsenges. Phys. Chem. **1968**, *72*, 257

(12) Yamazaki, Y.; Takeda, H.; Ishitani, O. **2015**, *25*, 106–137.

(13) Arias-Rotondo, D. M.; McCusker, J. K. *Chem. Soc. Rev.* **2016**, *45*, 5803–5820.

(14) Wasielewski, M. R. *Chem. Rev.* **1992**, *92*, 435–461.

(15) Zhang, X.; Yu, L.; Zhuang, C.; Peng, T.; Li, R.; Li, X. *ACS Catal.* **2014**, *4*, 162-170.

(16) Ueno, K.; Misawa, H. *NPG Asia Mater.* **2013**, *5* , e61.

(17) Fabian, J.; Nakazumi, H.; Matsuoka, M. *Chem. Rev.* **1992**, *92*, 1197–1226.

(18) Qian, G.; Wang, Z. Y. *Chem. - An Asian J.* **2010**, *5*, 1006–1029.

(19) Tsuda, A.; Osuka, A. *Science* **2001**, *293*, 79–83.

(20) Pschirer, N. G.; Kohl, C.; Nolde, F.; Qu, J.; Müllen, K. *Angew. Chem. Int. Ed.* **2006**, *45*, 1401–1404.

(21) Creutz, C.; Taube, H. *J. Am. Chem. Soc.* **1969**, *91*, 3988–3989.

(22) Zhao, W.; Carreira, E. M. *Angew. Chem. Int. Ed.* **2005**, *44*, 1677–1679.

(23) Zhu, X.; Tsuji, H.; Nakabayashi, K.; Ohkoshi, S. I.; Nakamura, E. *J. Am. Chem. Soc.* **2011**, *133*, 16342–16345.

(24) Fujitsuka, M.; Ohsaka, T.; Majima, T. *Phys. Chem. Chem. Phys.* **2015**, *17*, 31030.

(25) La Porte, N. T.; Martinez, J.; Hedström, S.; Rudshteyn, B.; Phelan, B. T.; Mauck, C. M.; Young, R. M.; Batista, V. S.; Wasielewski, M. R. *Chem. Sci.* **2017**, *8*, 3821.

(26) Zatsikha, Y. V.; Didukh, N. O.; Nemez, D.; Schlachter, A. C.; Karsenti, P.-L.; Kovtun, Y. P.; Harvey, P. D.; Nemykin, V. N. *Chem. Commun.* **2017**, *53*, 7612.

(27) Tsuji, Y.; Yamamoto, K.; Yamauchi, K.; Sakai, K. *Angew. Chem. Int. Ed.* **2018**, *57*, 208.

(28) Lu, C.; Fujitsuka, M.; Sugimoto, A.; Majima, T. *J. Phys. Chem. C* **2016**, *120*, 12734.

(29) Kudisch, B.; Maiuri, M.; Blas-Ferrando, V. M.; Ortiz, J.; Sastre-Santos, A.; Scholes, G. *Phys. Chem. Chem. Phys.* **2017**, *19*, 21078.

(30) Yusa, M.; Nagata, T. *Photochem. Photobiol. Sci.* **2017**, *16*, 1043.

(31) Shao, S.; Gobeze, H. B.; Karr, P. A.; D'Souza, F. *Chem. Asian J.* **2017**, *12*, 2258.

(32) Bandi, V.; El-Khouly, M. E.; Ohkubo, K.; Nesterov, V. N.; Zandler, M. E.; Fukuzumi, S.; D'Souza, F. *J. Phys. Chem. C* **2014**, *118*, 2321.

(33) Jiménez, A. J.; Grimm, B.; Gunderson, V. L.; Vagnini, M. T.; Krick Calderon, S.; Rodríguez-Morgade, M. S.; Wasielewski, M. R.; Guldi, D. M.; Torres, T. *Chem. Eur. J.* **2011**, *17*, 5024.

(34) Maligaspe, E.; Pundsack, T. J.; Albert, L. M.; Zatsikha, Y. V.; Solntsev, P. V.; Blank, D. A.; Nemykin, V. N. *Inorg. Chem.* **2015**, *54*, 4167.

(35) Zatsikha, Y. V.; Didukh, N. O.; Blesener, T.; Kayser, M. P.; Kovtun, Y. P.; Blank, D. A.; Nemykin, V. N. *Eur. J. Inorg. Chem.* **2017**, *2017*, 318.

(36) Zatsikha, Y. V.; Maligaspe, E.; Purchel, A. A.; Didukh, N. O.; Wang, Y.; Kovtun, Y. P.; Blank, D. A.; Nemykin, V. N. *Inorg. Chem.* **2015**, *54*, 7915.

(37) Whittemore, T. J.; Sayre, H. J.; Xue, C.; White, T. A.; Gallucci, J. C.; Turro, C. *J. Am. Chem. Soc.* **2017**, *139*, 14724.

(38) Fujitsuka, M.; Kim, S. S.; Lu, C.; Tojo, S.; Majima, T. *J. Phys. Chem. B* **2015**, *119*, 7275.

(39) Liu, J.-Y.; Hou, X.-N.; Tian, Y.; Jiang, L.; Deng, S.; Röder, B.; Ermilov, E. A. *RSC Adv.* **2016**, *6*, 57293.

(40) Haviv, E.; Shimon, L. J. W.; Neumann, R. *Chem. Eur. J.* **2017**, *23*, 92.

(41) Ermilov, E. A.; Liu, J.-Y.; Menting, R.; Huang, Y.-S.; Roder, B.; Ng, D. K. P. *Phys. Chem. Chem. Phys.* **2016**, *18*, 10964.

(42) Ermilov, E. A.; Liu, J. Y.; Ng, D. K. P.; Röder, B. *Phys. Chem. Chem. Phys.* **2009**, *11*, 6430.

(43) Blas-Ferrando, V. M.; Ortiz, J.; Bouissane, L.; Ohkubo, K.; Fukuzumi, S.; Fernández-Lázaro, F.; Sastre-Santos, Á. *Chem. Commun.* **2012**, *48*, 6241.

(44) Martín-Gomis, L.; Rotas, G.; Ohkubo, K.; Fernández-Lázaro, F.; Fukuzumi, S.; Tagmatarchis, N.; Sastre-Santos, Á. *Nanoscale* **2015**, *7*, 7437.

(45) Davis, C. M.; Ohkubo, K.; Ho, I.-T.; Zhang, Z.; Ishida, M.; Fang, Y.; Lynch, V. M.; Kadish, K. M.; Sessler, J. L.; Fukuzumi, S. *Chem. Commun.* **2015**, *51*, 6757.

(46) Bandi, V.; El-Khouly, M. E.; Ohkubo, K.; Nesterov, V. N.; Zandler, M. E.; Fukuzumi, S.; D'Souza, F. *Chem. Eur. J.* **2013**, *19*, 7221.

(47) Bandi, V.; Gobeze, H. B.; Nesterov, V. N.; Karr, P. A.; D'Souza, F. *Phys. Chem. Chem. Phys.* **2014**, *16*, 25537.

(48) Amin, A. N.; El-Khouly, M. E.; Subbaiyan, N. K.; Zandler, M. E.; Supur, M.; Fukuzumi, S.; D'Souza, F. *J. Phys. Chem. A* **2011**, *115*, 9810.

(49) Honda, T.; Kojima, T.; Fukuzumi, S. *Chem. Commun.* **2011**, *47*, 7986.

(50) El-Khouly, M. E.; Moiseev, A. G.; Van Der Est, A.; Fukuzumi, S. *Chem. Phys. Chem.* **2012**, *13*, 1191.

(51) Molina, D.; El-Khouly, M. E.; El-Kemary, M.; Fukuzumi, S.; Fernández-Lázaro, F.; Sastre-Santos, Á. *Chem. Eur. J.* **2016**, *22*, 17800.

(52) Isosomppi, M.; Tkachenko, N. V.; Efimov, A.; Vahasalo, H.; Jukola, J.; Vainiotalo, P.; Lemmetyinen, H. *Chem. Phys. Lett.* **2006**, *430*, 36.

(53) Pla, S.; Niemi, M.; Martín-Gomis, L.; Fernández-Lázaro, F.; Lemmetyinen, H.; Tkachenko, N. V. *Phys. Chem. Chem. Phys.* **2016**, *3598*, 3598.

(54) Martín-Gomis, L.; Peralta-Ruiz, F.; Thomas, M. B.; Fernández-Lázaro, F.; D'Souza, F.; Sastre-Santos, Á. *Chem. Eur. J.* **2017**, *23*, 3863.

(55) KC, C. B.; Lim, G. N.; D'Souza, F. *Nanoscale* **2015**, *7*, 6813.

(56) Eggenspiller, A.; Takai, A.; El-Khouly, M. E.; Ohkubo, K.; Gros, C. P.; Bernhard, C.; Goze, C.; Denat, F.; Barbe, J. M.; Fukuzumi, S. *J. Phys. Chem. A* **2012**, *116*, 3889.

(57) Shibano, Y.; Umeyama, T.; Matano, Y.; Tkachenko, N. V.; Lemmetyinen, H.; Imahori, H. *Org. Lett.* **2006**, *8*, 4425.

(58) Céspedes-Guirao, F. J.; Ohkubo, K.; Fukuzumi, S.; Fernández-Lázaro, F.; Sastre-Santos, Á. *Chem. Asian J.* **2011**, *6*, 3110.

(59) Bandi, V.; Gobeze, H. B.; D'Souza, F. *Chem. Eur. J.* **2015**, *21*, 11483.

(60) Obondi, C. O.; Lim, G. N.; Karr, P. A.; Nesterov, V. N.; D'Souza, F. *Phys. Chem. Chem. Phys.* **2016**, *18*, 18187.

(61) Gobeze, H. B.; Bandi, V.; D'Souza, F. *Phys. Chem. Chem. Phys.* **2014**, *16*, 18720.

(62) Shao, S.; Gobeze, H. B.; Karr, P. A.; D'Souza, F. *Chem. Eur. J.* **2015**, *21*, 16005.

(63) Gobeze, H. B.; Tram, T.; Chandra B, K. C.; Cantu, R. R.; Karr, P. A.; D'Souza, F. *Chinese J. Chem.* **2016**, *34*, 969.

(64) Bandi, V.; Souza, F. P. D.; Gobeze, H. B.; Souza, F. D. *Chem. Commun.* **2016**, *52*, 579.

(65) Bandi, V.; D'Souza, F. P.; Gobeze, H. B.; D'Souza, F. *Chem. Eur. J.* **2015**, *21*, 2669.

(66) Chandra B, K. C.; Lim, G. N.; D'Souza, F. *Chem. Eur. J.* **2016**, *22*, 13301.

(67) El-Khouly, M. E.; Gutiérrez, A. M.; Sastre-Santos, Á.; Fernández-Lázaro, F.; Fukuzumi, S. *Phys. Chem. Chem. Phys.* **2012**, *14*, 3612.

(68) Bandi, V.; El-Khouly, M. E.; Nesterov, V. N.; Karr, P. A.; Fukuzumi, S.; D'Souza, F. *J. Phys. Chem. C* **2013**, *117*, 5638.

(69) Jiménez, Á. J.; Sekita, M.; Caballero, E.; Marcos, M. L.; Rodríguez-Morgade, M. S.; Guldi, D. M.; Torres, T. *Chem. Eur. J.* **2013**, *19*, 14506.

(70) Liu, J. Y.; El-Khouly, M. E.; Fukuzumi, S.; Ng, D. K. P. *ChemPhysChem* **2012**, *13*, 2030.

(71) Shi, W. J.; El-Khouly, M. E.; Ohkubo, K.; Fukuzumi, S.; Ng, D. K. P. *Chem. Eur. J.* **2013**, *19*, 11332.

(72) El-Khouly, M. E.; Fukuzumi, S. *Photochem. Photobiol. Sci.* **2016**, *15*, 1340.

(73) Jiménez, Á. J.; Spănig, F.; Rodríguez-Morgade, M. S.; Ohkubo, K.; Fukuzuml, S.; Guldi, D. M.; Torres, T. *Org. Lett.* **2007**, *9*, 2481.

(74) Rotas, G.; Martín-Gomis, L.; Ohkubo, K.; Fernández-Lázaro, F.; Fukuzumi, S.; Tagmatarchis, N.; Sastre-Santos, Á. *Chem. Eur. J.* **2016**, *22*, 15137.

(75) Bonin, J.; Robert, M. *Photochem. Photobiol.* **2011**, *87*, 1190–1203.

(76) Dau, H.; Zaharieva, I. *Acc. Chem. Res.* **2009**, *42*, 1861–1870.

(77) Lennox, J. C.; Kurtz, D. A.; Huang, T.; Dempsey, J. L. *ACS Energy Lett.* **2017**, *2*, 1246–1256.

(78) Pannwitz, A.; Wenger, O. S. *J. Am. Chem. Soc.* **2017**, *139*, 13308–13311.

(79) Chararalambidis, G.; Das, S.; Trapali, A.; Quaranta, A.; Orio, M.; Halime, Z.; Fertey, P.; Guillot, R.; Coutsolelos, A.; Leibl, W.; Aukauloo, A.; Sircoglou, M. *Angew. Chem. Int. Ed.* **2018**, *57*, 9013–9017.

(80) Weinberg, D. R.; Gagliardi, C. J.; Hull, J. F.; Murphy, C. F.; Kent, C. A.; Westlake, B. C.; Paul, A.; Ess, D. H.; McCafferty, D. G.; Meyer, T. J. *Chem. Rev.* **2012**, *112*, 4016–4093.

(81) Warren, J. J.; Tronic, T. a.; Mayer, J. M. *Chem. Rev.* **2010**, *110*, 6961–7001.

(82) Reece, S. Y.; Nocera, D. G. *Annu. Rev. Biochem.* **2009**, *78*, 673–699.

(83) Mayer, J. M.; Hrovat, D. A.; Thomas, J. L.; Borden, W. T. *J. Am. Chem. Soc.* **2002**, *124*, 11142–11147.

(84) Michaudel, Q.; Kottisch, V.; Fors, B. P. *Angew. Chem. Int. Ed.* **2017**, *56*, 9670–9679.

(85) Adzima, B. J.; Tao, Y.; Kloxin, C. J.; DeForest, C. A.; Anseth, K. S.; Bowman, C. N. *Nat. Chem.* **2011**, *3*, 256–259.

(86) Gates, B. D.; Xu, Q.; Stewart, M.; Ryan, D.; Willson, C. G.; Whitesides, G. M. *Chem. Rev.* **2005**, *105*, 1171–1196.

(87) Hardy, M. D.; Konetski, D.; Bowman, C. N.; Devaraj, N. K. *Org. Biomol. Chem.* **2016**, *14*, 5555–5558.

(88) Budin, I.; Devaraj, N. K. *J. Am. Chem. Soc.* **2012**, *134*, 751–753.

Chapter 1

Near-IR Light-Induced Electron Transfer via Dynamic Quenching

INTRODUCTION

Photoinduced electron transfer (PET) reaction is one of the key processes in solar energy conversion reactions both in natural[1-3] and artificial systems[4-6]. Of particular interest is the development of PET reaction driven by near-infrared (NIR) light (> 700 nm), which accounts for more than 40% of the solar energy reaching on the earth, due to potential applications of the reaction, such as dye sensitized solar cells[7,8] and artificial photosynthesis[9,10], in addition to its fundamental importance[11,12]. In this context, extensive efforts have been devoted to construct PET systems using NIR absorbing compounds including Ru[13] and Rh complexes[14], phthalocyanines[15-17], BODIPYs[18,19], and some organic radicals[20,21]. However, most of these studies have demonstrated the PET systems driven by visible light (≤ 700 nm), and there are only a few reports on NIR light-induced electron transfer (NIR-ET) systems. Furthermore, all the reports on NIR-ET systems are limited to static quenching systems, in which a photosensitizer (PS) and a quencher (Q) must be assembled at their ground states[22-24]. The development of NIR-ET systems based on dynamic quenching, in which PS and Q do not have to associate with each other at the gourd state[25-27] and thus systematic investigation with various combinations of PS and Q is allowed, must broaden diversity of PET systems, and lay the foundation for the research field.

In this work, we succeeded in establishing the NIR-ET system with dynamic quenching. The key to the success is the finding of an excellent NIR-sensitizer, which exhibits strong NIR absorption, high photostability, and long excitation lifetime. We employed a distorted phthalocyanine (DPc) derivative as a photosensitizer (Chart 1). Although DPc derivatives are known to exhibit intense absorption in the NIR region[28,29], no example of NIR-ET systems using DPcs has been reported. Described here are the evaluation of physical properties of DPc derivatives as NIR photosensitizers, and the development of a NIR-ET system based on dynamic quenching.

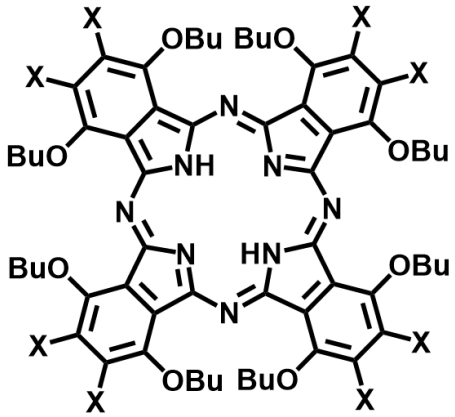

DPc-H (X = H)
DPc-Cl (X = Cl)

Chart 1. Molecular structures of the studied DPcs.

RESULTS AND DISCUSSION

Synthesis, Characterization and Properties of DPc-H

Our investigation started with the evaluation of the simplest DPc derivative, 1,4,8,11,15,18,22,25-octabutoxyphthalocyanine[30,31] (**DPc-H**, Chart 1), as a NIR photosensitizer. The synthesis of **DPc-H** was performed according to modified literature methods,[31] and the obtained compound was characterized by ^{1}H-NMR spectroscopy, elemental analysis, and X-ray crystallography (see Experimental Section for details). **DPc-H** has a saddle-like distorted structure due to steric effects between the butoxy substituents at the α-positions (Figure 1, Table 1)[31,32]. The distortion angles of the phthalocyanine ring are 24.3(4)° and 21.3(4)°. **DPc-H** exhibits intense absorption bands in the NIR region (Figure 2, λ_{max} = 769 nm and $\varepsilon = 1.3 \times 10^5$ $M^{-1}cm^{-1}$), which are assigned to e_g(LUMO) ← a_{1u}(HOMO) transitions (Q-bands), and moderately intense bands in the UV-Visible region (λ_{max} = 332 nm and $\varepsilon = 5.2 \times 10^4$ $M^{-1}cm^{-1}$), corresponding to e_g(LUMO) ← a_{2u}(HOMO−1) transitions (Soret bands)[30]. The Q-bands of **DPc-H** are largely redshifted compared to those of the planer phthalocyanine derivatives (typically, λ_{max} = 650–670 nm)[33] due to the distortion of the phthalocyanine ring[28,29]. Upon photoirradiation (150 W, 300–1400 nm, halogen lamp), however, the intensity of the band drastically decreased under aerobic conditions (Figure 3), which indicates the photodegradation of **DPc-H**. Actually, **DPc-H** is easily oxidized at −0.03 V (*vs*. ferrocene/ferrocenium (Fc/Fc^+)), suggesting the high HOMO level of the compound (Figure 4). It should be also noted that the photodegradation of **DPc-H** is largely suppressed in the absence of air (Figure 5). These results demonstrate that **DPc-H** decomposes via an oxidative pathway as common phthalocyanine compounds[34] and is not stable under photoirradiated conditions.

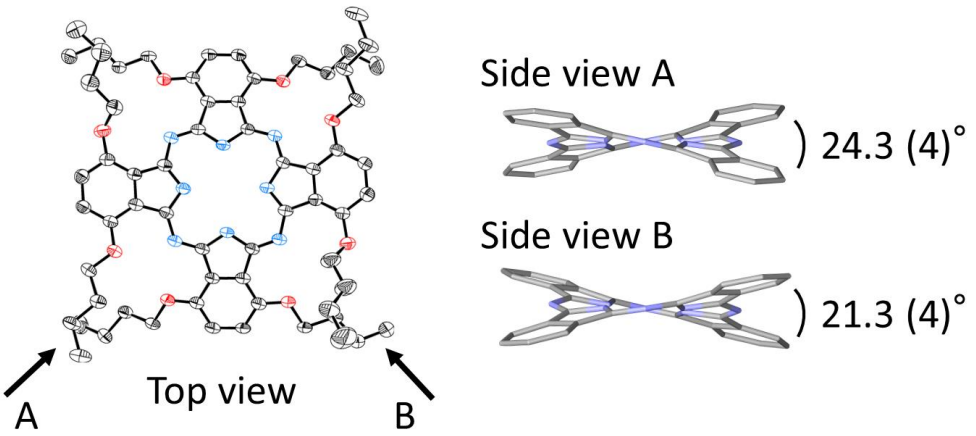

Figure 1. (Left) An ORTEP drawing (50% probability ellipsoids) of DPc-H. Hydrogen atoms and disordered butyl chains are omitted for clarity. (Right) Side views of DPc-H. Hydrogen atoms and butoxy groups are omitted for clarity. N = blue, O = red, C = grey.

Table 1. Summary of crystallographic data for **DPc-H**.

Formula	$C_{64}H_{82}N_8O$
Formula weight	1091.38
Crystal system	triclinic
Space group	$P\bar{1}$
a, Å	13.3946(7)
b, Å	14.0581(6)
c, Å	16.8681(8)
α, deg	72.4810(11)
β, deg	87.9920(12)
γ, deg	76.6960(11)
V, Å^3	2945.7(2)
Z	2
R_1	0.0741
wR_2	0.2516
GOF	0.995

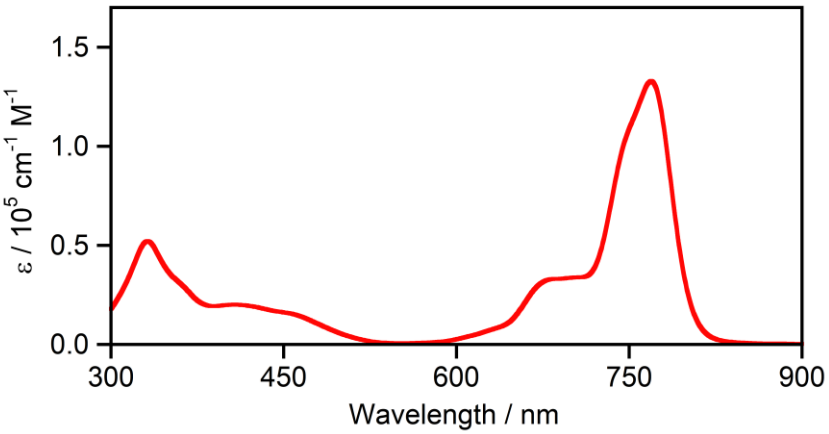

Figure 2. UV-Vis-NIR absorption spectrum of **DPc-H** in *o*-DCB.

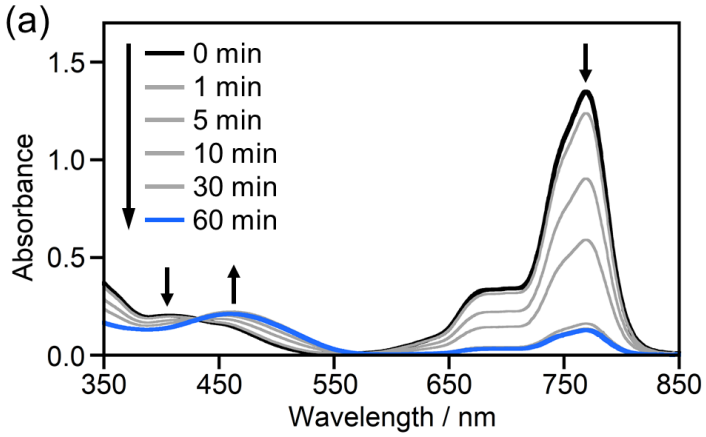

Figure 3. **DPc-H** in aerated *o*-DCB (10 μM) upon light irradiation by a halogen lamp (150 W, 300–1400 nm).

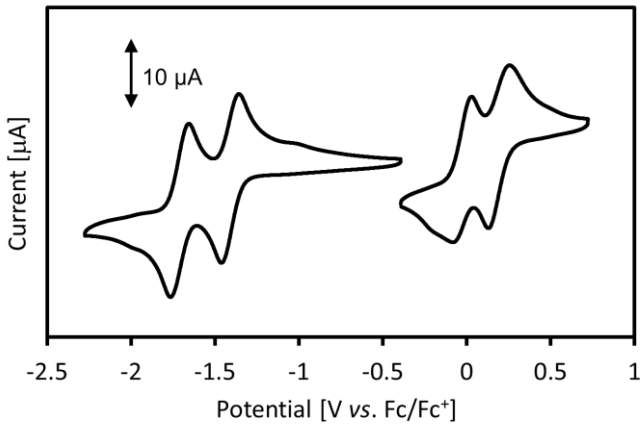

Figure 4. Cyclic voltammograms of **DPc-H** in *o*-DCB (supporting electrolyte: tetra-n-butylammonium perchlorate, WE:GC, scan rate:10 mV/s).

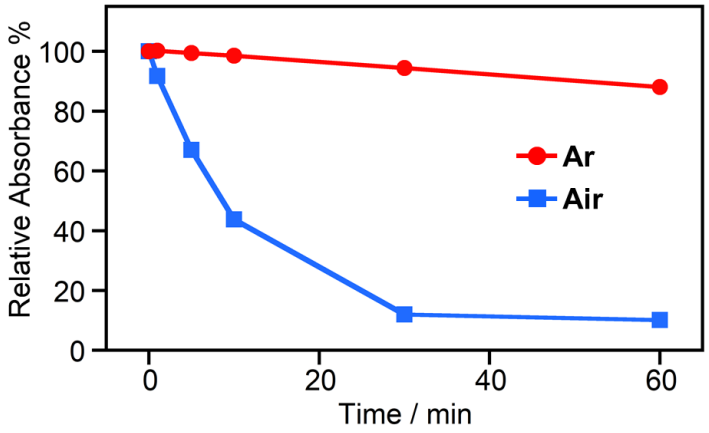

Figure 5. Plots of the changes in the absorption spectra of **DPc-H** during the photostability test under an aerobic condition (blue line) and Ar (red line). Relative changes in the absorbance of **DPc-H** were calculated from the change in absorbance at 769 nm. Experiments were performed using a solution of **DPc-H** in *o*-DCB (10 μM). The sample solution was irradiated by a halogen lamp (150 W, 300–1400 nm).

Synthesis, Characterization and Properties of DPc-Cl

Based on the aforementioned results, we subsequently employed a DPc derivative with electron-withdrawing chloro substituents at the *β*-positions, 1,4,8,11,15,18,22,25-octabutoxy-2,3,9,10,16,17,23,24-octachlorophthalocyanine (**DPc-Cl**, Chart 1) to increase the photostability. The synthesis of **DPc-Cl** was performed according to modified literature methods[31] (see Supporting Information for details). **DPc-Cl** also exhibits a saddle-like distorted structure similar to **DPc-H** (Figure 6, Table 2), and the distortion angles of the phthalocyanine ring are 18.2(8)° and 19.1(6)° [35]. As shown in Figure 7, **DPc-Cl** displays intense Q-bands in the NIR region (λ_{max} = 760 nm and ε = 1.5 × 10^5 $M^{-1}cm^{-1}$) and moderately intense Soret bands in the UV-Visible region (λ_{max} = 333 nm and ε = 5.0 × 10^4 $M^{-1}cm^{-1}$)[30]. No obvious shift of the Q-bands was observed between **DPc-H** and **DPc-Cl**, which suggests that the introduction of chloro substituents does not significantly affect the NIR absorption properties.

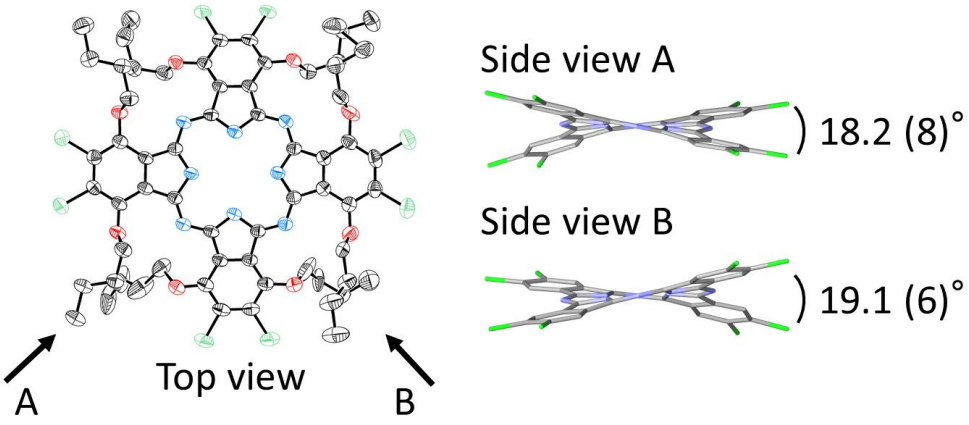

Figure 6. (Left) An ORTEP drawing (50% probability ellipsoids) of **DPc-Cl**. Hydrogen atoms and disordered butyl chains are omitted for clarity. (Right) Side views of **DPc-Cl**. Hydrogen atoms and butoxy groups are omitted for clarity. N = blue, O = red, C = grey, Cl = green.

Table 2. Summary of crystallographic data for **DPc-Cl**.

Formula	$C_{64}H_{74}Cl_8N_8O_8$
Formula weight	1366.91
Crystal system	triclinic
Space group	$P\bar{1}$
a, Å	15.1107(5)
b, Å	15.9844(7)
c, Å	16.3595(6)
α, deg	108.8990(10)
β, deg	93.8190(8)
γ, deg	114.7330(10)
V, Å^3	3300.2(2)
Z	2
R_1	0.0633
wR_2	0.218
GOF	1.006

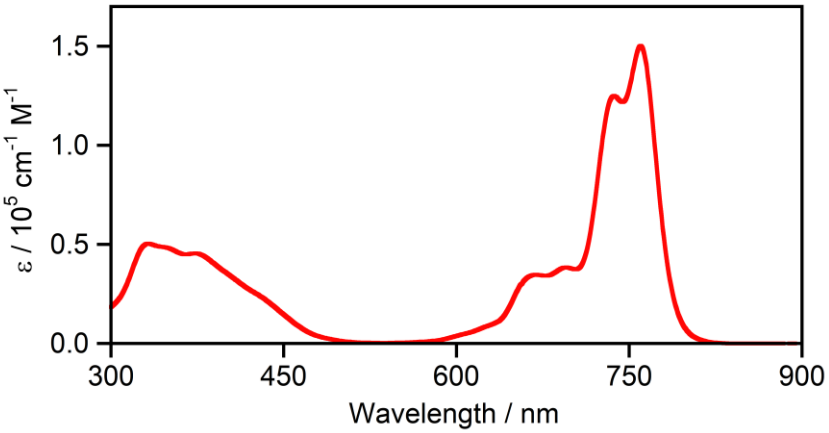

Figure 7. UV-Vis-NIR absorption spectrum of **DPc-Cl** in *o*-DCB.

Photostability Test of DPc-Cl

The photostability of **DPc-Cl** was studied under identical conditions as **DPc-H** (*vide supra*). In contrast to **DPc-H**, the UV-Vis-NIR absorption spectrum of **DPc-Cl** did not show an obvious change after 60 minutes of photoirradiation both under aerobic and Ar conditions (Figures 8 and 9). The decomposition ratios of **DPc-Cl** and **DPc-H** in the air were calculated to be < 1% and > 90%, respectively, based on the changes in the intensity of the Q-bands (Figure 10). This drastic difference in the photostability of the DPcs can be interpreted by considering their oxidation potentials. As shown in Figure 11, **DPc-Cl** displayed two reversible oxidation waves (0.43 and 0.66 V for **DPc-Cl** vs. Fc/Fc^{+}) and two reversible reduction waves (−1.50 and −1.13 V for **DPc-Cl**). The first oxidation potential of **DPc-Cl** (0.43 V) was shifted to the positive region by +0.46 V compared with that of **DPc-H** (−0.03 V). These results clearly reveal that the introduction of electron-withdrawing chloro substituents lowers the HOMO level of **DPc-Cl**, which prevents the photodegradation of the dye via oxidative pathway and affords its high photostability.

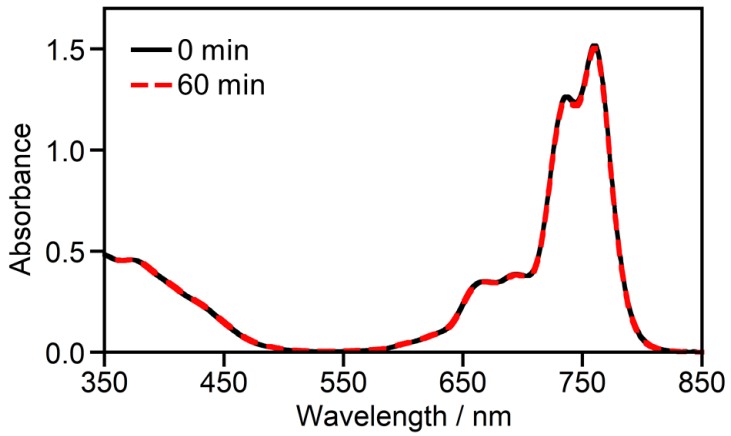

Figure 8. **DPc-Cl** in aerated *o*-DCB (10 μM) upon light irradiation by a halogen lamp (150 W, 300–1400 nm).

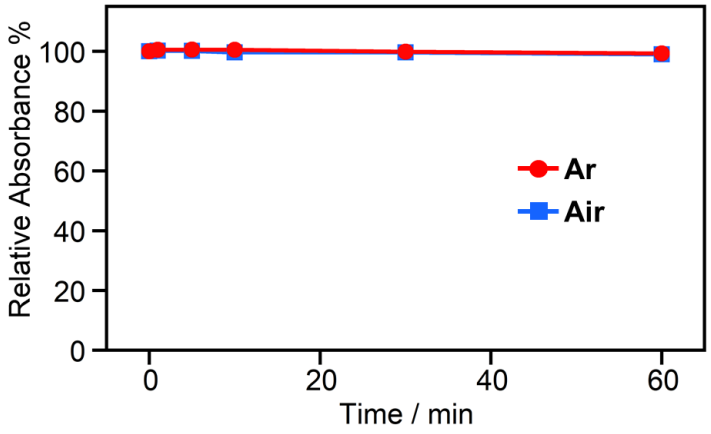

Figure 9. Plots of the changes in the absorption spectra of **DPc-Cl** during the photostability test under an aerobic condition (blue line) and Ar (red line). Relative changes in the absorbance of **DPc-Cl** were calculated from the change in absorbance at 761 nm. Experiments were performed using a solution of **DPc-Cl** in *o*-DCB (10 μM). The sample solution was irradiated by a halogen lamp (150 W, 300–1400 nm).

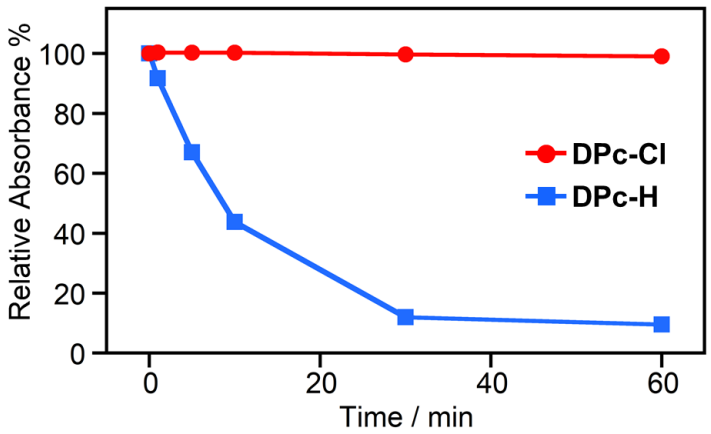

Figure 10. Plots of the changes in the absorption spectra of the DPcs during the photostability test under an aerobic condition. Relative changes in the absorbance of the DPcs were calculated from the change in absorbance at 761 nm for **DPc-Cl** and at 769 nm for **DPc-H**.

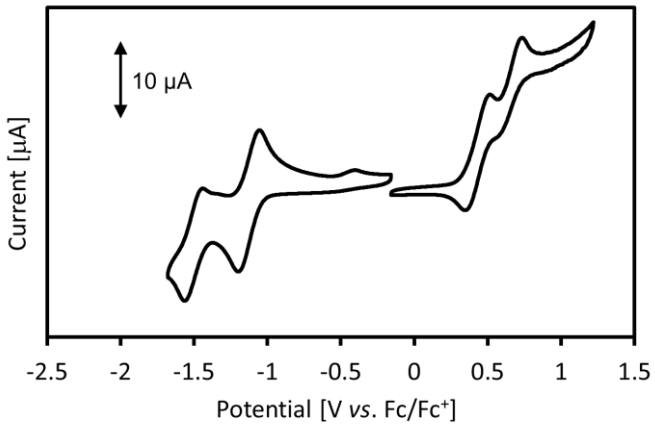

Figure 11. Cyclic voltammograms of **DPc-H** (black line) and **DPc-Cl** (red line) in *o*-DCB (supporting electrolyte: tetra-*n*-butylammonium perchlorate, WE:GC, scan rate:10 mV/s).

Lifetime Studies of DPc-Cl

To further investigate the photochemical properties of **DPc-Cl**, transient absorption spectroscopic measurements were conducted. Figure 12 displays the transient absorption spectrum of **DPc-Cl** in *o*-DCB under Ar atmosphere. After laser excitation at 430 nm, bleaching of the bands around 760 nm, attributed to **DPc-Cl**, and the emergence of a band around at 575 nm, assignable to the excited state of **DPc-Cl**, **DPc-Cl***, were observed. The absorbance time profile at 575 nm (Figure 13, λ_{ex} = 650 nm) exhibits a single exponential decay, and the lifetime of **DPc-Cl*** was estimated to be 40 μs. The lifetime of **DPc-Cl*** significantly decreased to 6 μs in the presence of O_2 (Figure 14). The result indicates that the long-lived excited state of **DPc-Cl** is a triplet state, which originated from the spin-orbit coupling of the conjugated aza-macrocyclic structure[36]. The lifetime of **DPc-Cl*** under anaerobic conditions (40 μs) is considered to be long enough to be utilized as a photosensitizer in dynamic quenching systems.[37]

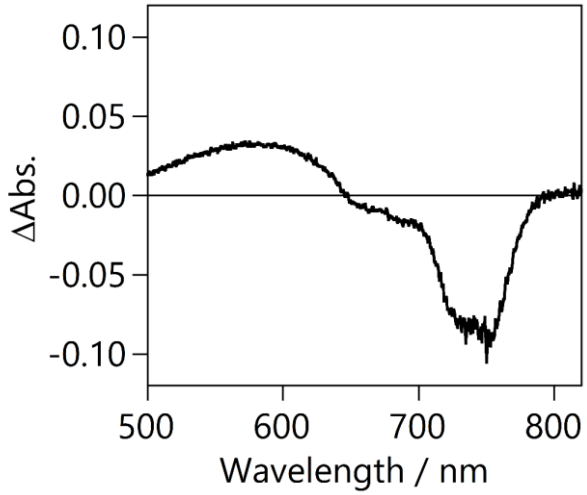

Figure 12. A transient absorption spectrum of **DPc-Cl** (10 μM) in *o*-DCB measured 1 μs after laser excitation at 430 nm.

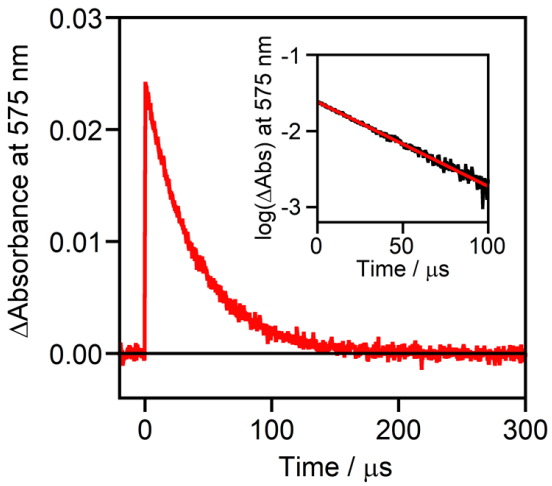

Figure 13. Absorbance time profile of **DPc-Cl** at 575 nm in *o*-DCB under Ar (λ_{ex} = 650 nm).

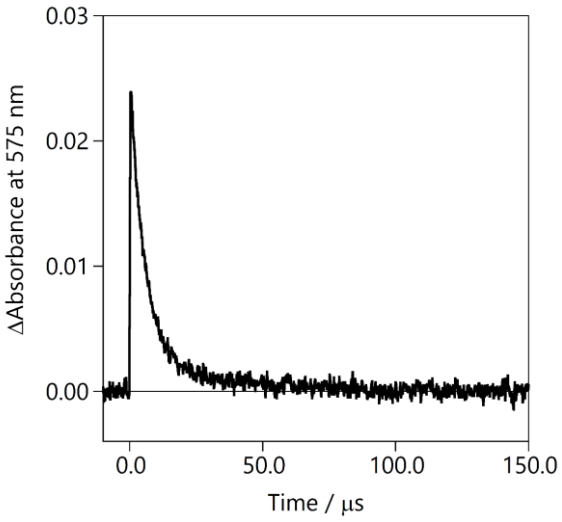

Figure 14. An absorbance time profile of **DPc-Cl** at 575 nm in *o*-DCB under air (λ_{ex} = 650 nm). Optical densities of the sample solution were 0.5 at 760 nm.

NIR-ET reaction using DPc-Cl

Encouraged by the aforementioned excellent properties of **DPc-Cl** as a NIR photosensitizer, i.e., its high stability and long-lived excited state, we explored the development of a NIR-ET system based on the dynamic quenching mechanism using **DPc-Cl** as a photosensitizer. An *o*-DCB solution containing **DPc-Cl** (10 μM) and 1,3-dimethyl-2-phenylbenzimidazoline (BIH, 1.0 mM) as a sacrificial electron donor was irradiated by NIR light (> 750 nm). Note that only Q-bands of **DPc-Cl**, which locate in the NIR region, can be excited in this experimental condition. As shown in Figure 15, the intensity of the Q-bands of **DPc-Cl** gradually decreased upon photoirradiation, and new peaks centered at 403, 621, 681, and 1083 nm appeared. During the spectral change, isosbestic points were observed at 392, 424, 456, 700, and 796 nm, which clearly indicates the conversion of **DPc-Cl** to a single product.

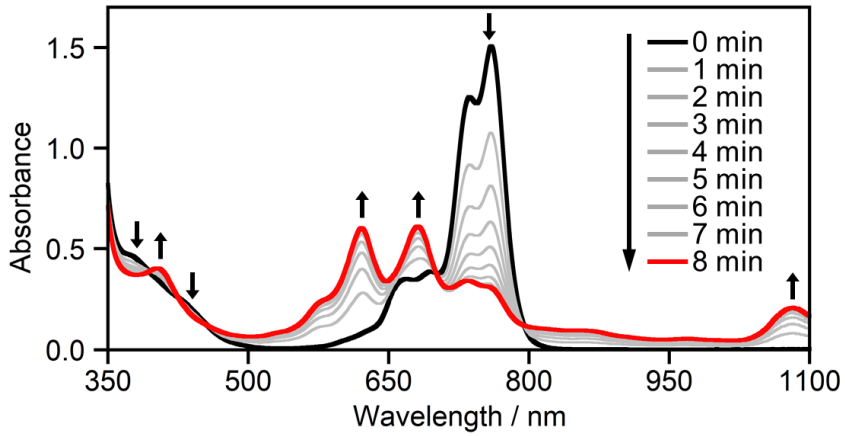

Figure 15. (a) Changes in the absorption spectra of **DPc-Cl** (10 μM) in *o*-DCB with BIH (1.0 mM) upon NIR light irradiation by a halogen lamp (150 W) with a long path filter (> 750 nm).

The details of the photoinduced reaction were investigated by several experiments. First, one electron reduced species of **DPc-Cl** were generated by chemical reduction using cobaltocene (Cp_2Co, $E_{1/2} = -1.21$ V vs. Fc^+/Fc)[38] as a chemical reductant. The UV-Vis-NIR absorption spectrum of the species generated by the chemical reduction is similar to that of the photochemically generated product (Figure 16). Subsequently, the solution after the photochemical reaction was investigated by X-band ESR spectroscopy. As shown in Figure 17, the solution gave an ESR signal at $g = 2.0034$ at 70 K, suggesting the formation of radical species. Therefore, the product of the photochemical reaction is best described as the radical anion of **DPc-Cl**, **DPc-Cl**$^{-\cdot}$. The conversion ratio of **DPc-Cl** to **DPc-Cl**$^{-\cdot}$ was roughly estimated to be 80% based on the steady-state results of the NIR photolysis.[39] We also evaluated the kinetics of the reaction by laser flash photolysis experiments. Absorbance time profiles of **DPc-Cl*** at 575 nm were recorded at various concentrations of BIH (0–5.0 mM), and the pseudo-first-order quenching constant (k_{obs}) under each condition was determined (Table 3). The value of k_{obs} linearly increased with increasing BIH concentration, and the quenching rate constant (k_q) of **DPc-Cl*** by BIH was estimated to be 1.0×10^6 $M^{-1}s^{-1}$ from the slope of the plot shown in Figure 18. In addition, the UV-Vis-NIR absorption spectrum of **DPc-Cl** did not change upon addition of BIH (Figure 19), indicating that there are no interactions between **DPc-Cl** and BIH at the ground state. These results clearly demonstrate **DPc-Cl** can serve as a photosensitizer to promote a NIR-ET reaction via the dynamic quenching mechanism described in Scheme 1. Additionally, we found that **DPc-Cl**$^{-\cdot}$ was relatively stable under inert atmosphere; the lifetime of **DPc-Cl**$^{-\cdot}$ generated by NIR irradiation was determined to be 8.5 min in dark conditions (Figures 20 and 21). This result indicates that the energy of the NIR light was stored as chemical energy in our system.

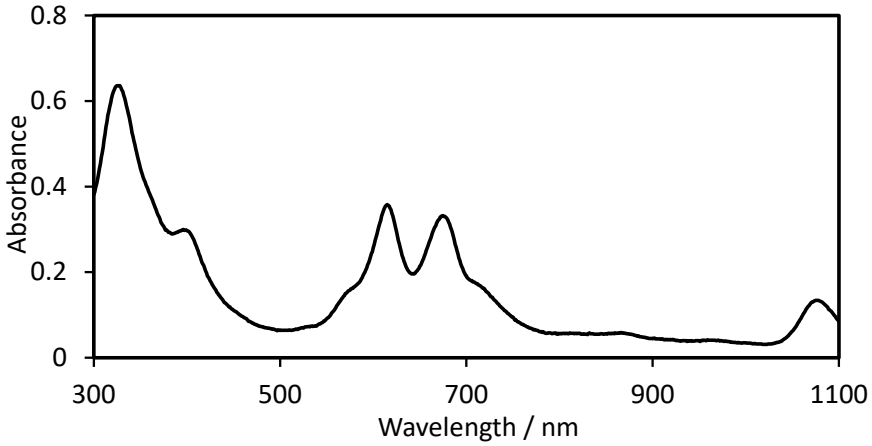

Figure 16. An absorption spectrum of **DPc-Cl** (5 μM) in THF in the presence of 20 eq. of $CoCp_2$ under Ar atmosphere.

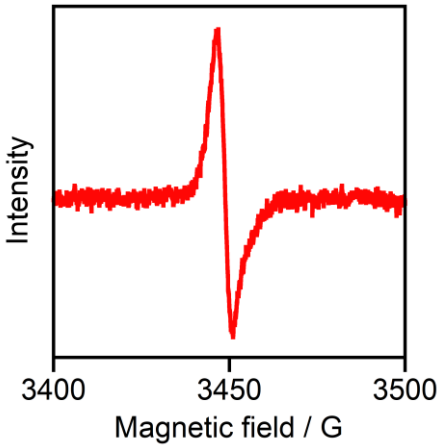

Figure 17. X-band ESR spectrum of the product obtained from the photochemical reaction. The measurement was performed at 70 K.

Table 3. Excitation lifetimes of **DPc-Cl** in the presence of various concentrations of BIH (0.0 – 5.0 mM) and pseudo-first-order quenching constants (k_{obs}) under each condition.

[Q] / mM	Lifetime / μs			k_{obs} (SD) / 10^4 s^{-1}
	Run 1	Run 2	Run 3	
5.0	32.88	32.37	33.50	3.04(5)
4.0	34.13	33.54	33.68	2.96(2)
3.0	34.51	34.83	35.39	2.87(3)
2.0	36.18	36.56	35.73	2.77(3)
1.0	37.84	37.63	37.59	2.653(9)
0.0	39.41	40.01	39.65	2.51(1)

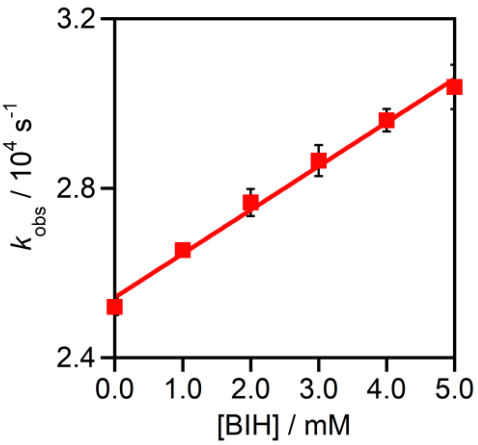

Figure 18. Plot of the pseudo-first-order rate constant (k_{obs}) for the NIR-ET reaction between **DPc-Cl** and BIH *vs* the concentration of BIH. Averaged k_{obs} values determined from the results of transient absorption spectroscopic measurements were shown as red squares with error bars. The measurements were performed for three times at each point. A sample solution was freshly prepared before each measurement.

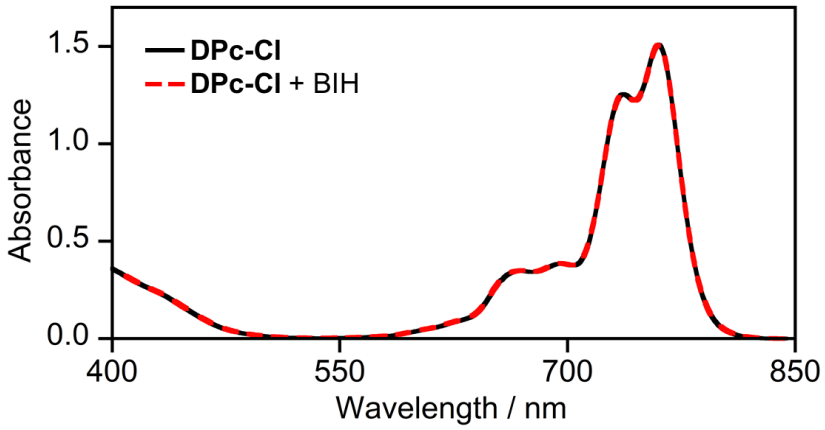

Figure 19. Absorption spectra of **DPc-Cl** (10 μM) in *o*-DCB in the absence and the presence of BIH (1 mM). Note that BIH does not have any absorption bands between 400 and 850 nm.

Scheme 1. Reaction schemes of NIR-ET reaction.

$$\mathbf{DPc\text{-}Cl} \xrightarrow[(> 750\ nm)]{\textit{NIR light}} \mathbf{DPc\text{-}Cl^{*}} \qquad (1)$$

$$\mathbf{DPc\text{-}Cl^{*} + BIH} \xrightarrow{\textit{ET}} \mathbf{DPc\text{-}Cl^{-\cdot} + BIH^{+\cdot}} \qquad (2)$$

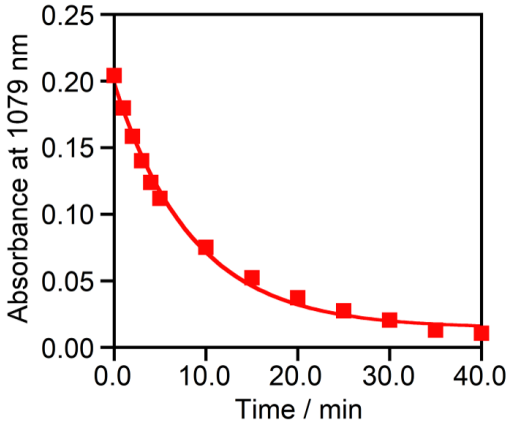

Figure 20. Absorbance time profile of **DPc-Cl**$^{\bullet-}$ generated by NIR irradiation under dark condition.

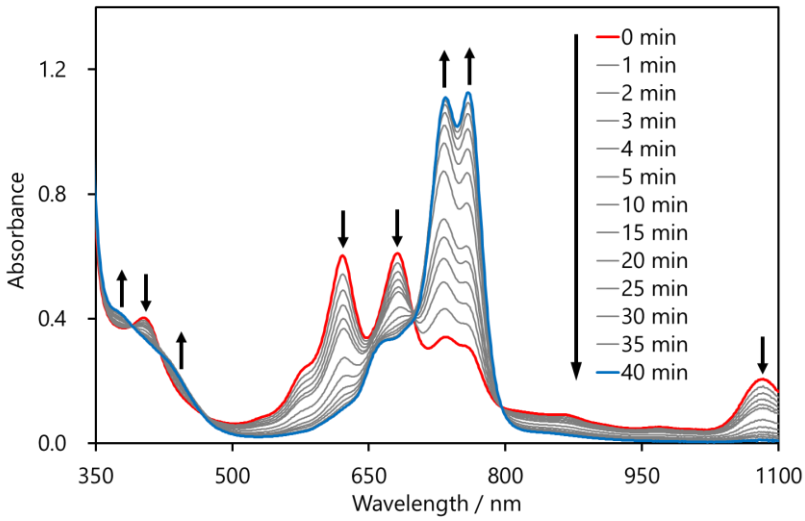

Figure 21. Changes in the absorption spectra of **DPc-Cl**$^{\bullet-}$ generated by NIR-ET reaction under dark condition.

CONCLUSION

In summary, we successfully developed a NIR-ET system based on a dynamic quenching mechanism for the first time. A distorted phthalocyanine derivative with electron-withdrawing groups, **DPc-Cl**, was revealed to exhibit high photostability and a long excitation lifetime for ET reactions. Using **DPc-Cl** as a NIR photosensitizer, an electron transfer reaction to generate the one-electron-reduced species of **DPc-Cl**, **DPc-Cl**$^{-\cdot}$, proceed under NIR light irradiation. The photochemically generated **DPc-Cl**$^{-\cdot}$ exhibits a substantially long lifetime. Moreover, mechanistic investigations indicated that our NIR-ET system is classified into a dynamic quenching system. Our results will pave the new way for the construction of energy conversion systems utilizing NIR light.

EXPERIMENTAL SECTION

Materials

K_2CO_3, $Na_2S_2O_5$, KOH, acetic acid, 1-bromobutane, ferrocene and all solvents were purchased from Wako Pure Chemical Industries, Ltd. 1-Butanol, 2,3-dicyanohydroquinone, tetra-*n*-butylammonium bromide, 1-iodobutane, *N*,*N*'-dimethyl-*o*-phenylenediamine, benzaldehyde and tetra-*n*-butylammonium perchlorate (TBAP) were purchased from Tokyo Chemical Industry Co., Ltd. Metal lithium was purchased from Kanto Chemical Co., Inc. 2,3-Dichloro-5,6-dicyano-1,4-benzoquinone and cobaltocene were purchased from Aldrich Chemical Co., Inc. All solvents and reagents were used as received, except for TBAP. TBAP was purified by recrystallization from ethanol and dried in vacuo. 3,6-Dibutoxy-1,2-benzenedicarbonitrile[40] and 3,6-dibutoxy-4,5-dichloro-1,2-benzenedicarbonitrile[30], the precursors of **DPc-H** and **DPc-Cl**, respectively, were prepared by the literature method. Compounds **DPc-H** and **DPc-Cl** were synthesized from the corresponding phthalonitriles according to the previous reports[30,31] with modifications. 1,3-Dimethyl-2-phenylbenzimidazoline (BIH) was also prepared by the literature method.[41]

Syntheses

Synthesis of 1,4,8,11,15,18,22,25-octabutoxyphthalocyanine (DPc-H)

A 50 mL flask containing 3,6-dibutoxy-1,2-benzenedicarbonitrile (272 mg, 1 mmol) and *n*-butanol (2 mL) was heated to 80 °C. After the complete dissolution of the dinitrile, chopped lithium metal (100 mg, 14 mmol) was slowly added to the vigorously stirred solution. After the complete addition of lithium, the mixture was heated to 120 °C and stirred under argon for 1 h. The reaction mixture was cooled to room temperature, diluted with acetic acid (20 mL), and filtered. The filtrate was stirred for 30 min, and water was added. The product was extracted from the reaction mixture with CH_2Cl_2. The extract was washed with several portions of equal volume of a saturated aqueous $NaHCO_3$ solution. Washing with bicarbonate was stopped once gas bubbles were no longer observed after mixing. The organic layer was collected, and dried with Na_2SO_4, and filtered. The filtrate

was reduced to dryness. The resulting solid was recrystallized from CH_2Cl_2/MeOH and from hot hexane to give **DPc-H** as a dark green solid (146 mg, 54%). ^{1}H NMR ($CDCl_3$): δ 7.59 (s, 8H), 4.84 (t, 16H, *J* = 8.0 Hz), 2.23 (sxt, 16H, *J* = 8.0 Hz), 1.66 (quin, 16H, *J* = 8.0 Hz), 1.08 (t, 24H, *J* = 7.2 Hz), 0.23 (s, 2H). Anal. Calcd for $C_{64}H_{82}N_8O_8$: C, 70.43; H, 7.57; N, 10.27. Found: C, 70.30; H, 7.45; N, 10.21.

Synthesis of 1,4,8,11,15,18,22,25-octabutoxy-2,3,9,10,16,17,23,24-octachloro-phthalocyanine (DPc-Cl)

A 100 mL flask containing 3,6-dibutoxy-4,5-dichloro-1,2-benzenedicarbonitrile (1.4 g, 4 mmol) and *n*-butanol (16 mL) was heated to 80 °C. After the complete dissolution of the dinitrile, chopped lithium metal (640 mg, 93 mmol) was slowly added to the vigorously stirred solution. After the complete addition of lithium, the mixture was heated to reflux and stirred under argon for 1 h. The reaction mixture was then cooled to room temperature and diluted with acetic acid (20 mL), and filtered. The filtrate was stirred for 30 min, a, and water was added. The product was extracted from the reaction mixture with CH_2Cl_2. The extract was washed with several portions of equal volume of a saturated aqueous $NaHCO_3$ solution. Washing with bicarbonate was stopped once gas bubbles were no longer observed after mixing. The organic layer was collected, and dried with Na_2SO_4, and filtered. The filtrate was reduced to dryness. The resulting solid was recrystallized from CH_2Cl_2/MeOH to give **DPc-Cl** as a light green solid (556 mg, 41%). ^{1}H NMR ($CDCl_3$): δ 4.94 (t, 16H, *J* = 8.0 Hz), 2.17 (sxt, 16H, *J* = 8.0 Hz), 1.64 (quin, 16H, *J* = 8.0 Hz), 1.03 (t, 24H, *J* = 8.0 Hz), 0.22 (s, 2H). Anal. Calcd for $C_{64}H_{74}N_8O_8Cl_8$: C, 56.23; H, 5.47; N, 8.22. Found: C, 56.49; H, 5.50; N, 8.20.

General Methods

^{1}H NMR spectra were acquired on a JEOL JNM-LA400 spectrometer, where chemical shifts in $CDCl_3$ were referenced to internal tetramethylsilane. Elemental analyses were carried out on a J-SCIENCE LAB MICRO CORDER JM10 elemental analyzer. UV-Vis-NIR absorption spectra were recorded on a Shimadzu UV-3600 UV-Vis-NIR spectrophotometer or UV-Vis Agilent Cary8454 spectrophotometer. Cyclic

voltammograms were measured at room temperature on a BAS ALS Model 650DKMP electrochemical analyzer in *o*-DCB (sample = 0.5 mM; 0.1 M tetra-*n*-butylammonium perchlorate (TBAP)). A glassy carbon disk, platinum wire, and Ag/Ag^+ electrode (Ag / 0.01 M $AgNO_3$) were used as the working, auxiliary, and reference electrodes, respectively. The redox potentials of samples were calibrated against the redox signal for the ferrocene/ferrocenium (Fc/Fc^+) couple. All electrochemical measurements were conducted under argon. Crystals of **DPc-H** and **DPc-Cl** were mounted in a loop. Diffraction data at 123 K were measured on a RAXIS-RAPID Imaging Plate diffractometer equipped with confocal monochromated Mo-Kα radiation and data was processed using RAPID-AUTO (Rigaku). The structure was solved by direct method using *SIR-92*[42] and refined by the full-matrix least squares techniques on F^2 (*SHELXL-97*[43]). All non-hydrogen atoms were refined anisotropically and refined with a riding model with U_{iso} constrained to be 1.2 times U_{eq} of the carrier atom. Molecular graphics were generated using *ORTEP*-3[44] for windows. Summary of crystallographic data for **DPc-H** and **DPc-Cl** are shown in Tables 1 and 2, respectively.

Transient Absorption Spectroscopy

The nanosecond flash photolysis experiments were carried out using a UNISOKU TSP-1000NL-01R nanosecond laser flash photolysis system. Sample solutions were excited with the third harmonic of a LS-2134UTF Nd:YAG laser (7-8 ns pulses, 10 Hz) with LT-2214OPO. Transient absorbance changes were monitored using an UNISOKU MD200 spectrometer and an USHIO UXL-75XE Xe lamp. The YAG lamp energy was 27 J.

Photochemical Reaction

Photochemical reactions were performed using a custom-made photoreactor with coolant to control the temperature of sample during photoreaction (Figure 22). All photoreactions were performed at 20 °C. For photostability test, *o*-DCB solutions of DPcs in quartz cell (10 x 10 x 30 mm^3, 3 mL) were irradiated by a halogen lamp (NPI PLL-150/7H-AL,150 W, 300 – 1400 nm) under air, and the reaction was monitored by the UV-Vis-NIR absorption spectral changes. In the case of the PET reaction, sample solutions in quartz

cell (10 x 10 x 30mm, 3 mL) were purged by Ar prior to the reaction and the solutions were irradiated by a halogen lamp with a long path filter (150 W, > 750 nm). The reaction was monitored by the UV-Vis-NIR absorption spectral changes.

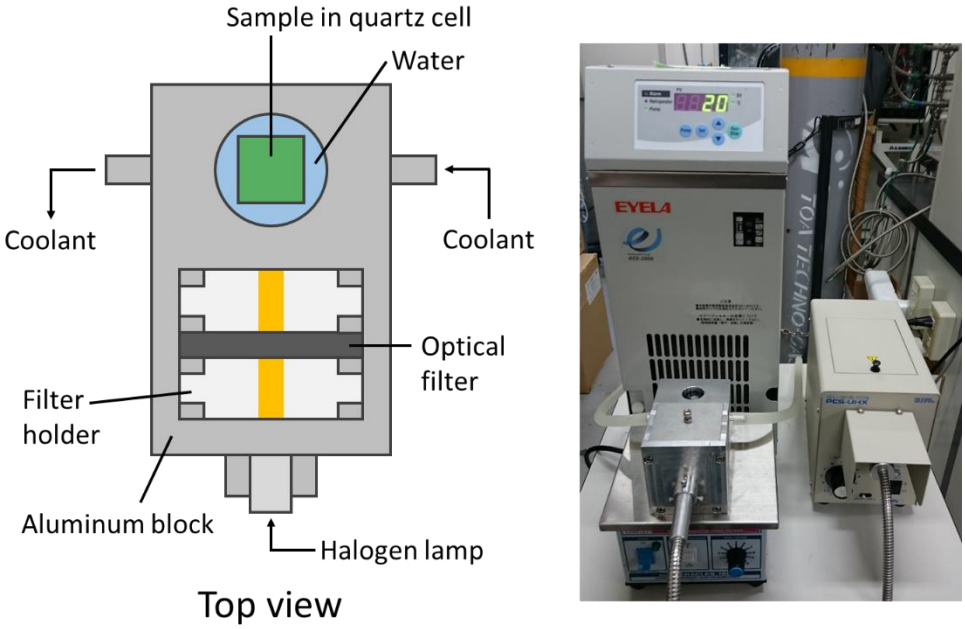

Figure 22. Schematic illustration of a custom-made photoreactor (left) and a photograph of the reactor (right).

Electron Spin Resonance Measurements

An X-band ESR spectrum of photochemically generated product of **DPc-Cl** were recorded on a Bruker E500 ESR spectrometer equipped with an Oxford ESR 900 cryostat for low-temperature measurements. The sample solution was prepared by the irradiation of NIR light (150 W, > 750 nm, 4 min) to a *o*-DCB solution of **DPc-Cl** (0.01 mM) in the presence of BIH (1 mM). The sample solution was immediately frozen by liquid N_2 after the NIR irradiation and the ESR measurement was carried out at 70K. ESR spectrum was obtained with following instrumental settings: microwave frequency 9.67 GHz, microwave power 0.1 mW, field modulation amplitude 1 G at 100 kHz, and time constant 164 ms.

REFERENCES

(1) Barber, J. *Chem. Soc. Rev.* **2009**, *38*, 185–196.

(2) Dau, H.; Zaharieva, I. *Acc. Chem. Res.* **2009**, *42*, 1861–1870.

(3) Ferreira, K. N.; Iverson, T. M.; Maghlaoui, K.; Barber, J.; Iwata, S. *Science* **2004**, *303*, 1831–1838.

(4) Nocera, D. G. *Acc. Chem. Res.* **2012**, *45*, 767–776.

(5) McConnell, I.; Li, G.; Brudvig, G. W. *Chem. Biol.* **2010**, *17*, 434–447.

(6) Tachibana, Y.; Vayssieres, L.; Durrant, J. R. *Nat. Photonics* **2012**, *6*, 511–518.

(7) Hagfeldt, A.; Boschloo, G.; Sun, L.; Kloo, L.; Pettersson, H. *Chem. Rev.* **2010**, *110*, 6595–6663.

(8) Kinoshita, T.; Nonomura, K.; Jeon, N. J.; Giordano, F.; Abate, A.; Uchida, S.; Kubo, T.; Seok, S. I.; Nazeeruddin, M. K.; Hagfeldt, A., et al. *Nat. Commun.* **2015**, *6*, 8834.

(9) Ueno, K.; Misawa, H. *NPG Asia Mater.* **2013**, *5*, e61.

(10) Zhang, X.; Yu, L.; Zhuang, C.; Peng, T.; Li, R.; Li, X. *ACS Catal.* **2014**, *4*, 162–170.

(11) El-Khouly, M. E.; Fukuzumi, S.; D'Souza, F. *ChemPhysChem* **2014**, *15*, 30–47.

(12) Jiménez, Á. J.; Calderón, R. M. K.; Rodríguez-Morgade, M. S.; Guldi, D. M.; Torres, T. *Chem. Sci.* **2013**, *4*, 1064–1074.

(13) Tsuji, Y.; Yamamoto, K.; Yamauchi, K.; Sakai, K. *Angew. Chem. Int. Ed.* **2018**, *57*, 208–212.

(14) Whittemore, T. J.; Sayre, H. J.; Xue, C.; White, T. A.; Gallucci, J. C.; Turro, C. *J. Am. Chem. Soc.* **2017**, *139*, 14724–14732.

(15) D'Souza, F.; Ito, O. *Chem. Soc. Rev.* **2012**, *41*, 86–96.

(16) Honda, T.; Kojima, T.; Fukuzumi, S. *Chem. Commun.* **2011**, *47*, 7986–7988.

(17) Yusa, M.; Nagata, T. *Photochem. Photobiol. Sci.* **2017**, *16*, 1043–1048.

(18) Bandi, V.; El-Khouly, M. E.; Ohkubo, K.; Nesterov, V. N.; Zandler, M. E.; Fukuzumi, S.; D'Souza, F. *J. Phys. Chem. C* **2014**, *118*, 2321–2332.

(19) Zatsikha, Y. V.; Maligaspe, E.; Purchel, A. A.; Didukh, N. O.; Wang, Y.; Kovtun, Y. P.; Blank, D. A.; Nemykin, V. N. *Inorg. Chem.* **2015**, *54*, 7915–7928.

(20) La Porte, N. T.; Martinez, J.; Hedström, S.; Rudshteyn, B.; Phelan, B. T.; Mauck, C. M.; Young, R. M.; Batista, V. S.; Wasielewski, M. R. *Chem. Sci.* **2017**, *8*, 3821–3831.

(21) Fujitsuka, M.; Kim, S. S.; Lu, C.; Tojo, S.; Majima, T. *J. Phys. Chem. B* **2015**, *119*, 7275–7282.

(22) Sauvage, J. P.; Collin, J. P.; Chambron, J. C.; Guillerez, S.; Coudret, C.; Balzani, V.; Barigelletti, F.; De Cola, L.; Flamigni, L. *Chem. Rev.* **1994**, *94*, 993–1019.

(23) Sun, L.; Hammarström, L.; Åkermark, B.; Styring, S. *Chem. Soc. Rev.* **2001**, *30*, 36–49.

(24) Sessler, J. L.; Jayawickramarajah, J.; Gouloumis, A.; Torres, T.; Guldi, D. M.; Maldonado, S.; Stevenson, K. J. *Chem. Commun.* **2005**, *14*, 1892–1894.

(25) Teets, T. S.; Nocera, D. G. *Chem. Commun.* **2011**, *47*, 9268–9274.

(26) You, Y.; Nam, W. *Chem. Soc. Rev.* **2012**, *41*, 7061–7084.

(27) Arias-Rotondo, D. M.; McCusker, J. K. *Chem. Soc. Rev.* **2016**, *45*, 5803–5820.

(28) Mack, J.; Kobayashi, N. *Chem. Rev.* **2011**, *111*, 281–321.

(29) Fukuda, T.; Homma, S.; Kobayashi, N. *Chem. Eur. J.* **2005**, *11*, 5205–5216.

(30) Fox, J. P.; Goldberg, D. P. *Inorg. Chem.* **2003**, *42*, 8181–8191.

(31) Gao, Y.; Chen, Y.; Li, R.; Bian, Y.; Li, X.; Jiang, J. *Chem. Eur. J.* **2009**, *15*, 13241–13252.

(32) The crystal data have been deposited at the Cambridge Crystallographic Data Centre (CCDC No. 1818387 for **DPc-H**). The crystal structure of **DPc-H** has been reported at 273K (reference 32).

(33) Claessens, C. G.; Hahn, U.; Torres, T. *Chem. Rec.* **2008**, *8*, 75–97.

(34) It is reported that some phthalocyanine derivatives decompose via an oxidative pathway in the presence of dioxygen. Słota, R.; Dyrda, G. *Inorg. Chem.* **2003**, *42*, 5743–5750.

(35) The crystal data have been deposited at the Cambridge Crystallographic Data Centre (CCDC No. 1817331 for **DPc-Cl**).

(36) Ishii, K.; Kobayashi, N. In *The Porphyrin Handbook Phthalocyanines: Spectroscopic and Electrochemical Characterization*; Kadish K., Guilard R., Smith, K. M., Eds.; Academic Press: New York, 2012; Vol. 16, pp1–42.

(37) For example, the excitation life time of $[Ru(bpy)_3]^{2+}$, a well-known photosensitizer utilized in several unorganized visible light induced ET reactions is 0.86 μs (in acetonitrile). Caspar, J. V.; Meyer, T. J. Photochemistry of $Ru(bpy)_3^{2+}$. Solvent Effects. *J. Am. Chem. Soc.* **1983**, *105*, 5583–5590.

(38) Connelly, N. G.; Geiger, W. E. *Chem. Rev.* **1996**, *96*, 877–910.

(39) The conversion ratio was calculated from the absorption spectral changes at 1083 nm, which is attributed to the absorption of **DPc-Cl**$^{\cdot-}$. The molar absorption coefficient of **DPc-Cl**$^{\cdot-}$ was estimated from the absorption spectrum of **DPc-Cl**$^{\cdot-}$ generated by chemical reduction (Fig. 16).

(40) Galanin, N. E.; Shaposhnikov, G. P. *Russ. J. Gen. Chem.* **2009**, *79*, 1024–1028.

(41) Naab, B. D.; Guo, S.; Olthof, S.; Evans, E. G. B.; Wei, P.; Millhauser, G. L.; Kahn, A.; Barlow, S.; Marder, S. R.; Bao, Z. *J. Am. Chem. Soc.* **2013**, *135*, 15018–15025.

(42) Altomare, A.; Cascarano, G.; Giacovazzo, C.; Guagliardi, A. *J. Appl. Crystallogr.* **1993**, *26*, 343–350.

(43) Sheldrick, G. M. *Acta Crystallogr. Sect.* **2007**, *64*, 112–122.

(44) Barnes, C. L. *J. Appl. Crystallogr.* **1997**, *30*, 568–568.

Chapter 2

Proton-Coupled Electron Transfer Induced by Near-Infrared Light

INTRODUCTION

Proton-coupled electron transfer (PCET) is a chemical process which involves simultaneous or stepwise transfer of electrons and protons, and plays an important role in many schemes of chemical and biological systems[1-6]. In particular, conjugation of PCET to photoinduced electron transfer (*i.e.*, photoinduced PCET) is of great significance because back electron transfer reaction can largely be suppressed in such a process.[7-9] Indeed, natural photosynthetic system realizes efficient photo-to-chemical energy conversions via the formation of a long-lived charge-separated state by using the photoinduced PCET reaction[10-12]. Inspired by the natural photosynthesis, extensive efforts have been made for developing artificial photoinduced PCET system, which aim not only to provide fundamental mechanistic understandings of the reactions[13-16] but also to construct efficient photo-to-chemical energy conversion systems[17-20]. However, investigation on artificial photoinduced PCET systems is still limited to the reactions induced by UV and visible light, and the development of PCET reactions induced by near-infrared (NIR) light (> 700 nm) remains a challenging objective. Given the fact that NIR light accounts for more than 40% of the solar energy reaching on the earth[21-23], the construction of a NIR light induced PCET system is essential to utilize solar energy with high efficiency. Herein the author reports the first example of NIR light induced PCET (NIR-PCET) system. In our NIR-PCET system, back electron transfer reaction was successfully suppressed and the formed radical species exhibited a relatively long lifetime. The author also confirmed the high reversibility and robustness of the system.

RESULTS AND DISCUSSION

To construct NIR-PCET system, the utilization of a dye molecule with following three requirements is essential; intense NIR absorption property, high electron transfer ability and proton accepting/donating capability. In this study, we hypothesized that the anionic species of a phthalocyanine derivative, 1,4,8,11,15,18,22,25-octabutoxy-2,3,9,10,16,17,23,24-octachloro-phthalocyaninato mono-anion (**1**$^{-}$, Scheme 1), can be a promising candidate as a dye molecule due to following reasons. First, phthalocyanine derivatives with bulky substituents at α-positions usually exhibit intense absorption bands in the NIR region due to their distorted structures[24,25]. Second, phthalocyanine derivatives generally undergo reversible electron transfer reactions owing to their large π-conjugated system[26] Third, inner imine groups of **1**$^{-}$ are expected to function as a proton association site.

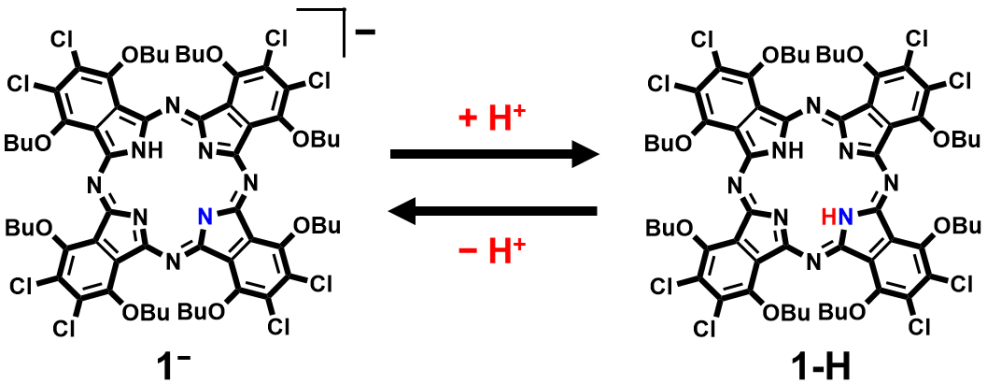

Scheme 1. Protonation / deprotonation equilibrium of **1**$^{-}$.

Generation and investigation on the physical properties of $\mathbf{1}^-$

Our study started with the generation and investigation on the physical properties of $\mathbf{1}^-$. The generation of $\mathbf{1}^-$ was examined by the deprotonation of its conjugate acid, **1-H**, using a base. Figure 1 shows the UV-vis-NIR absorption spectral changes of **1-H** in *o*-dichlorobenzene (*o*-DCB) upon addition of 1,8-diazabicyclo[5.4.0]undec-7-ene (DBU). The absorption spectral titration resulted in the bleaching of the absorption bands of **1-H** centred at 373 and 760 nm and the generation of new peaks centred at 722 and 425 nm associated with isosbestic points at 736, 673, 665 and 407 nm. The result indicates that $\mathbf{1}^-$ can be generated by the deprotonation of **1-H**, and $\mathbf{1}^-$ exhibits intense absorption bands in the NIR region. A Hill plot obtained from the titration also clarified that one proton is dissociated from **1-H** upon addition of the base to form $\mathbf{1}^-$ (Figure 2, see experimental section for details). Furthermore, the proton association constant of $\mathbf{1}^-$ was estimated to be $K = 8.1 \times 10^{-4}$, confirming the proton accepting ability of $\mathbf{1}^-$. A cyclic voltammogram of $\mathbf{1}^-$ showed one reversible reduction wave at −1.26 V (vs. Ag/Ag^+, Figure 3), indicating the electron transfer ability of $\mathbf{1}^-$. From these results, it is concluded that $\mathbf{1}^-$ has all three features required for a dye to be utilized in NIR-PCET system.

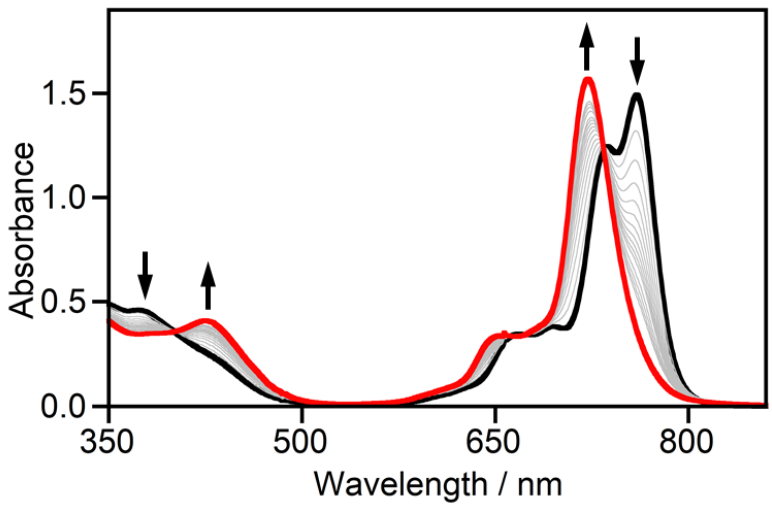

Figure 1. Absorption spectral changes in the course of titration of **1-H** (10 μM) in *o*-DCB with DBU (0 – 44 mM).

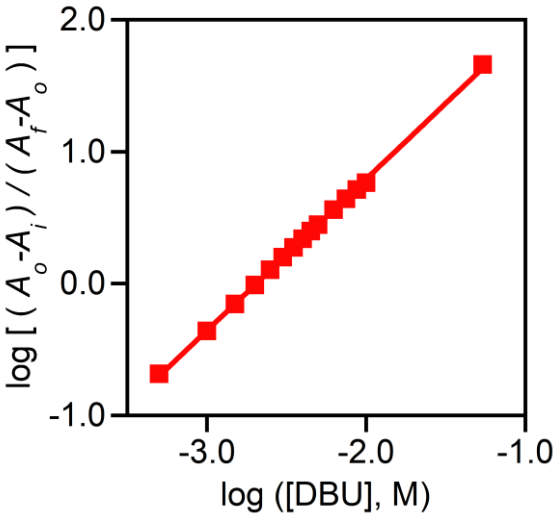

Figure 2. A Hill plot to determine the stoichiometry and the formation constant.

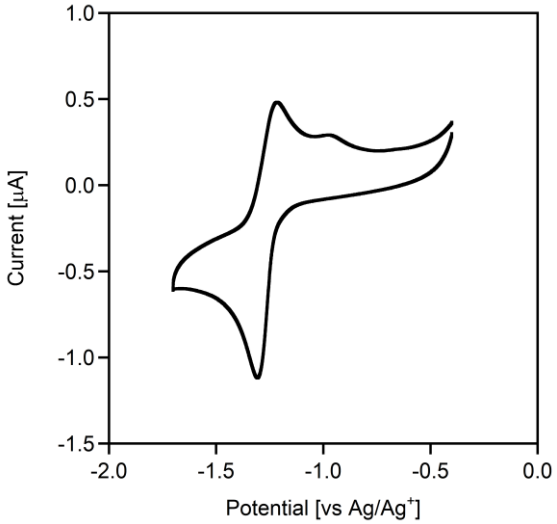

Figure 3. Cyclic voltammogram of $\mathbf{1}^-$ (0.5 mM) in 0.1 M TBAP/o-DCB under Ar in the presence of 5 M DBU. Working electrode, glassy carbon; counter electrode, Pt wire; reference electrode, Ag/Ag^+; scan rate, 10 mVs^{-1}.

NIR-PCET reaction using $\mathbf{1}^-$

Subsequently, photoreactivity of $\mathbf{1}^-$ upon NIR light irradiation was investigated in the presence of sacrificial electron donor and water. Initially, $\mathbf{1}^-$ was generated by adding trimethylamine (TEA) as a base to a THF/water mixed solution (4:1 v/v) of **1-H** containing sodium ascorbate (NaAsc) as a sacrificial electron donor. Irradiation of NIR light (> 710 nm) to the solution purged by Ar resulted in the absorption spectral changes shown in Figure 4. The absorption peaks originated from $\mathbf{1}^-$ gradually decreased upon the NIR light irradiation, and new peaks were observed at 400 nm, 616 nm, 675 nm and 1078 nm. During this absorption spectral changes, isosbestic points were observed at 411 nm, 477 nm, 690 nm and 780 nm, which indicates the formation of a single product from $\mathbf{1}^-$. The absorption spectrum of the solution after the irradiation of NIR light for 8 min was almost identical to that of one-electron reduced species of **1-H** ($\mathbf{1\text{-}H}^{-\cdot}$) generated by chemical reduction by cobaltocene (Figure 4, blue dashed line). These results clearly demonstrate that $\mathbf{1}^-$ is directly converted to $\mathbf{1\text{-}H}^{-\cdot}$ via the transfer of one electron and one proton upon irradiation of the NIR light. In other words, $\mathbf{1}^-$ can undergo a NIR-PCET reaction to afford $\mathbf{1\text{-}H}^{-\cdot}$ as a single product. The conversion ratio from $\mathbf{1}^-$ to $\mathbf{1\text{-}H}^{-\cdot}$ was estimated to be 90% based on the results of the steady-state results of the NIR photolysis.[27] It was also found that photochemically generated $\mathbf{1\text{-}H}^{-\cdot}$ is stable under dark condition, and the rate of the reverse reaction is quite small; the lifetime of $\mathbf{1\text{-}H}^{-\cdot}$ under dark condition was estimated to be 5.2 min (Figures 5,6). In contrast, $\mathbf{1}^-$ was rapidly regenerated when the solution was exposed to air (Figure 7). The result indicates that the oxidation of $\mathbf{1\text{-}H}^{-\cdot}$ by O_2 and the subsequent release of proton regenerates $\mathbf{1}^-$. Further irradiation of the NIR light to the resultant solution after purging Ar again generated $\mathbf{1\text{-}H}^{-\cdot}$, confirming the reversibility of the conversion reaction between $\mathbf{1}^-$ and $\mathbf{1\text{-}H}^{-\cdot}$. Additionally, after 4 cycles of conversion reactions, 99% of $\mathbf{1}^-$ remained[28], which suggests high stability of our NIR-PCET system. These findings clearly demonstrate that our NIR-PCET system can generate stable species, $\mathbf{1\text{-}H}^{-\cdot}$ by supressing back electron transfer reaction, and exhibits high reversibility and durability.

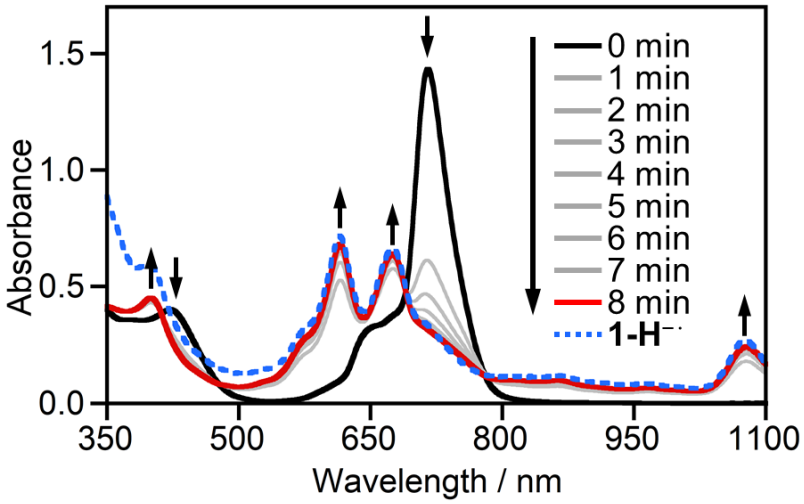

Figure 4. Changes in the absorption spectrum of $\mathbf{1}^-$ (10 μM) in deaerated THF/H_2O (4:1 v/v) solution with TEA (100 mM) and NaAsc (5 mM) upon NIR light irradiation by a halogen lamp (150 W) with a long path filter (>710 nm). Dashed line: An absorption spectrum of **DPc-Cl** (5 μM) in THF in the presence of 20 eq. of $CoCp_2$ under Ar atmosphere.

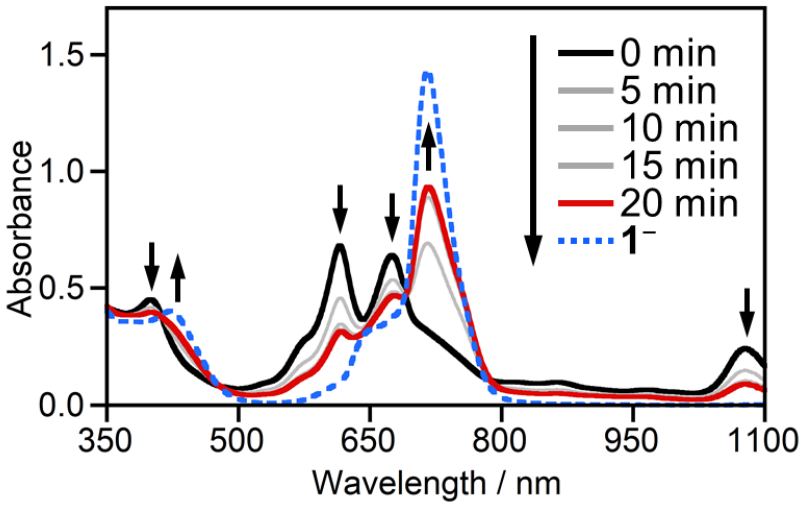

Figure 5. Changes in the absorption spectra of $\mathbf{1\text{-}H}^{-\cdot}$ generated by NIR-ET reaction in dark condition.

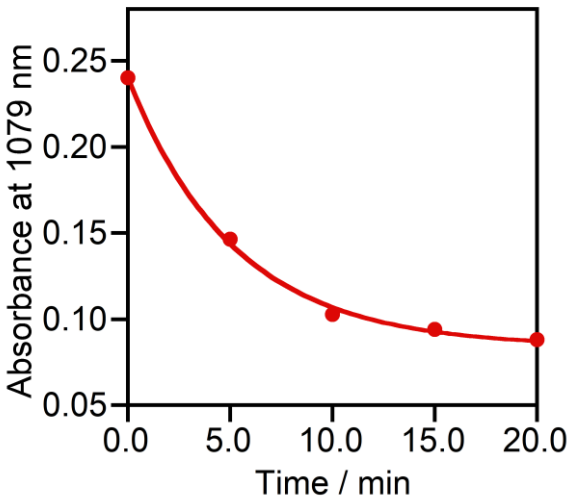

Figure 6. Time course of the decay of **1-H**$^{-\cdot}$ generated by NIR-ET reaction in dark condition.

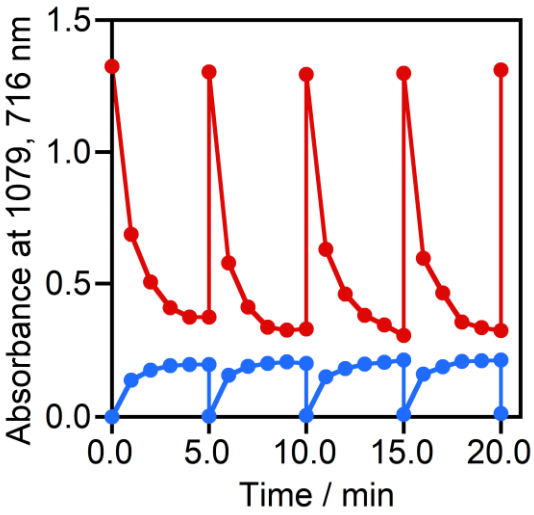

Figure 7. Repeated absorption spectral changes of **1**$^{-}$ (10 μM) in THF/H2O (4:1) with NaAsc (5 mM) and TEA (100 mM) at 716 nm (red line) and 1079 nm (blue line) in the course of NIR light irradiation (>710 nm, 5 min / cycle) under Ar atmosphere and subsequent air exposure.

H/D kinetic isotope effect

The H/D kinetic isotope effect (KIE) on the formation of **1-H**$^{-\cdot}$ was investigated to further understand the reaction mechanism of our NIR-PCET system. Figure 8 shows the absorption spectral changes of **1**$^{-}$ upon photoirradiation in THF/D_2O in the presence of NaAsc. Similar to the reaction in THF/H_2O (Figure 4), spectral changes with the isosbestic points were observed and the new bands attributed to the **1-D**$^{-\cdot}$ was observed (Figure 8). However, the time courses of the absorption at 1079 nm is largely different between the reactions in THF/H_2O and THF/D_2O; the absorption spectral changes in the presence of D_2O is more sluggish than that in the presence of H_2O (Figure 9). The result clearly shows that the formation of **1-D**$^{-\cdot}$ was slower than that of **1-H**$^{-}$, and thus, the transfer of the proton is involved in the rate determining step in our NIR-PCET system.

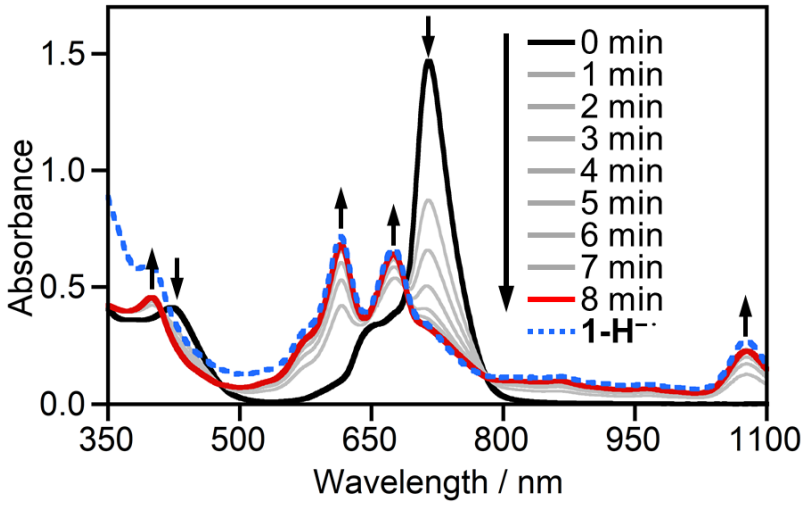

Figure 8. Changes in the absorption spectra of **1**$^{-}$ (10 μM) in deaerated THF/D_2O (4:1 v/v) solution with TEA (100 mM) and NaAsc (5 mM) upon NIR light irradiation by a halogen lamp (150 W) with a long path filter (>710 nm). Dashed line: absorption spectrum of **1-H**$^{-\cdot}$ generated by chemical reduction using cobaltocene.

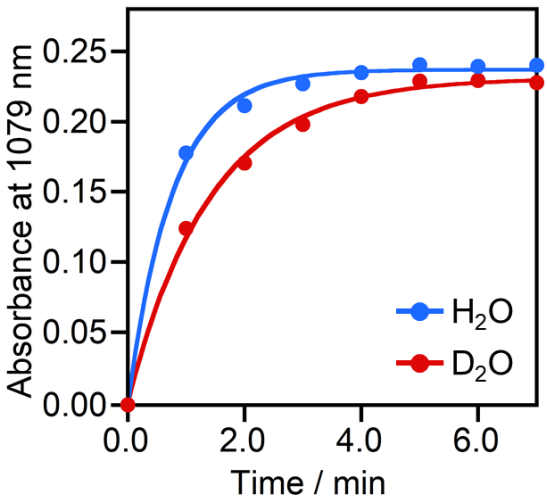

Figure 9. Time course of the generation of **1-H**$^{-\cdot}$ or **1-D**$^{-\cdot}$ upon NIR light irradiation of deaerated THF/H_2O (4:1 v/v) or THF/D_2O (4:1 v/v) solution containing **1**$^-$ (10 μM), TEA (100 mM) and NaAsc (5 mM).

CONCLUSION

In summary, a photoinduced PCET system driven by NIR light was successfully established for the first time, using $\mathbf{1}^{-}$, which exhibits intense NIR absorption property and electron transfer and proton accepting abilities. UV-vis absorption spectroscopic measurements revealed that that our NIR-PCET system can generate long-lived radical species by suppressing a back electron transfer reaction and exhibited high reversibility and robustness. Moreover, the transfer of the proton is involved in the rate determining step of the reaction as evidenced by the investigation of the H/D kinetic isotope effect (KIE) on the formation of $\mathbf{1\text{-}H}^{-\cdot}$. These results will pave the way for the applications of PCET reaction driven by low energy photons.

EXPERIMENTAL SECTION

Materials

1,4,8,11,15,18,22,25-Octabutoxy-2,3,9,10,16,17,23,24-octachloro-phthalocyanine (**1-H**) were synthesized according to literature procedure[29] All the solvents were purchased from Wako Pure Chemical Industries, while the chemicals were purchased from Tokyo Chemical Industry Co., Ltd., Sigma-Aldrich Co., Kanto Chemical Co., Inc., and Wako Pure Chemical Industries. All the reagents were of highest quality available and were used as received.

General Methods

^{1}H-NMR spectra were collected at room temperature on a JEOL JNM-ECS400 spectrometer. UV-vis absorption spectra were measured on a UV-Vis Agilent Cary8454 spectrophotometer at room temperature. Elemental analyses were performed on a J-Science Lab Micro Corder JM10 elemental analyzer.

Determination of a Proton Association Constant of $\mathbf{1}^-$

The proton association constant of $\mathbf{1}^-$ (K, eq. 1) was determined using Hill equation (eq. 2).

$$\textbf{1-H} + \textbf{TEA} \underset{}{\overset{K}{\rightleftharpoons}} \mathbf{1}^- + \textbf{H-TEA}^+ \quad (1)$$

$$\log\left(\frac{A_\mathrm{o} - A_i}{A_\mathrm{f} - A_o}\right) = n\log[\mathrm{TEA}] + \log\frac{1}{K} \quad (2)$$

A_o is observed absorbance, A_i is an absorbance of **1-H**, A_f is an absorbance of $\mathbf{1}^-$, n is a number of proton to react, and [TEA] is the concentration of TEA. Hill equation analyzes changes of absorption spectra during the titration as a function of the concentration of added base.

Photochemical Reaction

Photochemical reactions were performed using a custom-made photoreactor with coolant to control the temperature of sample during photoreaction (Figure 10). All photoreactions were performed at 20 °C. Sample solutions in quartz cell (10 x 10 x 30mm, 3 mL) were purged by Ar prior to the reaction and the solutions were irradiated by a halogen lamp with a long path filter (150 W, > 710 nm). The reaction was monitored by the UV-Vis-NIR absorption spectral changes.

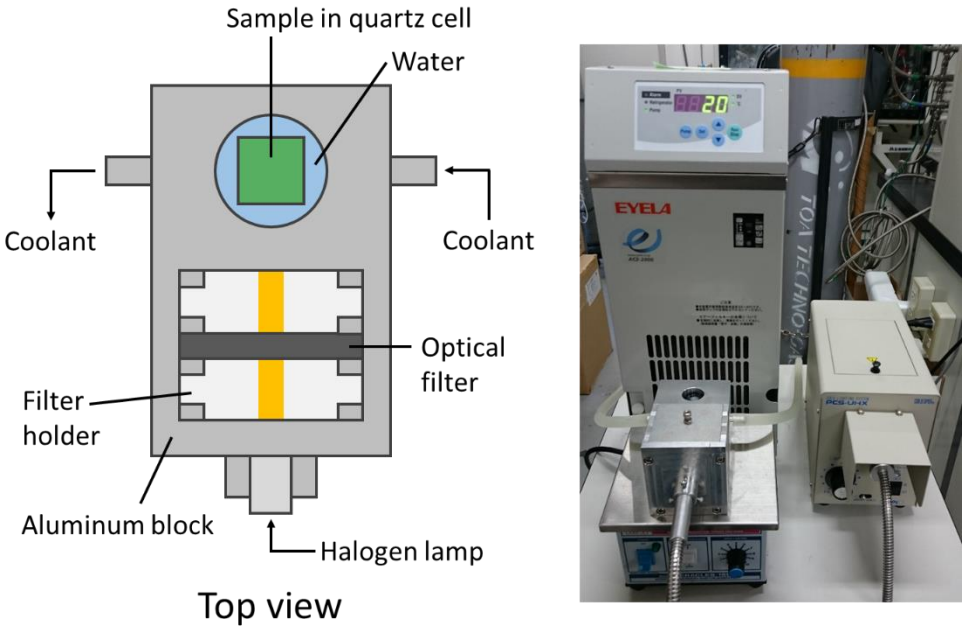

Figure 10. Schematic illustration of a custom-made photoreactor (left) and a photograph of the reactor (right).

REFERENCES

(1) Weinberg, D. R.; Gagliardi, C. J.; Hull, J. F.; Murphy, C. F.; Kent, C. A.; Westlake, B. C.; Paul, A.; Ess, D. H.; McCafferty, D. G.; Meyer, T. J. *Chem. Rev.* **2012**, *112*, 4016–4093.

(2) Hammes-Schiffer, S. *J. Am. Chem. Soc.* **2015**, *137*, 8860–8871.

(3) Gagliardi, C. J.; Vannucci, A. K.; Concepcion, J. J.; Chen, Z.; Meyer, T. J. *Energy Environ. Sci.* **2012**, *5*, 7704–7717.

(4) Warren, J. J.; Tronic, T. a.; Mayer, J. M. *Chem. Rev.* **2010**, *110*, 6961–7001.

(5) Suga, M.; Akita, F.; Sugahara, M.; Kubo, M.; Nakajima, Y.; Nakane, T.; Yamashita, K.; Umena, Y.; Nakabayashi, M.; Yamane, T.; Nakano, T.; Suzuki, M.; Masuda, T.; Inoue, S.; Kimura, T.; Nomura, T.; Yonekura, S.; Yu, L. J.; Sakamoto, T.; Motomura, T.; Chen, J. H.; Kato, Y.; Noguchi, T.; Tono, K.; Joti, Y.; Kameshima, T.; Hatsui, T.; Nango, E.; Tanaka, R.; Naitow, H.; Matsuura, Y.; Yamashita, A.; Yamamoto, M.; Nureki, O.; Yabashi, M.; Ishikawa, T.; Iwata, S.; Shen, J. R. *Nature* **2017**, *543*, 131–135.

(6) Reece, S. Y.; Nocera, D. G. *Annu. Rev. Biochem.* **2009**, *78*, 673–699.

(7) Goyal, P.; Hammes-Schiffer, S. *ACS Energy Lett.* **2017**, *2*, 512–519.

(8) Meyer, T. J.; Huynh, M. H. V.; Thorp, H. H. *Angew. Chemie - Int. Ed.* **2007**, *46*, 5284–5304.

(9) Hattori, Y.; Abdellah, M.; Rocha, I.; Pavliuk, M. V.; Fernandes, D. L. A.; Sá, J.

(10) Bonin, J.; Robert, M. *Photochem. Photobiol.* **2011**, *87*, 1190–1203.

(11) Dau, H.; Zaharieva, I. *Acc. Chem. Res.* **2009**, *42*, 1861–1870.

(12) Barber, J. *Chem. Soc. Rev.* **2009**, *38*, 185–196.

(13) Wenger, O. S. *Coord. Chem. Rev.* **2015**, *282–283*, 150–158.

(14) Dongare, P.; Bonn, A. G.; Maji, S.; Hammarström, L. *J. Phys. Chem. C* **2017**, *121*, 12569–12576.

(15) Oliver, T. A. A.; Zhang, Y.; Roy, A.; Ashfold, M. N. R.; Bradforth, S. E. *J. Phys. Chem. Lett.* **2015**, *6*, 4159–4164.

(16) Nomrowski, J.; Wenger, O. S. *Inorg. Chem.* **2015**, *54*, 3680–3687.

(17) Pannwitz, A.; Wenger, O. S. *J. Am. Chem. Soc.* **2017**, *139*, 13308–13311.

(18) Chararalambidis, G.; Das, S.; Trapali, A.; Quaranta, A.; Orio, M.; Halime, Z.; Fertey, P.; Guillot, R.; Coutsolelos, A.; Leibl, W.; Aukauloo, A.; Sircoglou, M. *Angew. Chem. Int. Ed.* **2018**, *57*, 9013–9017.

(19) Natali, M.; Amati, A.; Demitri, N.; Iengo, E. *Chem. Commun.* **2018**, *54*, 6148–6152.

(20) Megiatto, J. D.; Antoniuk-Pablant, A.; Sherman, B. D.; Kodis, G.; Gervaldo, M.; Moore, T. A.; Moore, A. L.; Gust, D. *Proc. Natl. Acad. Sci.* **2012**, *109*, 15578–15583.

(21) Kinoshita, T.; Nonomura, K.; Jeon, N. J.; Giordano, F.; Abate, A.; Uchida, S.; Kubo, T.; Seok, S. Il; Nazeeruddin, M. K.; Hagfeldt, A.; Grätzel, M.; Segawa, H. *Nat. Commun.* **2015**, *6*, 8834.

(22) Bai, Y.; Olivier, J. H.; Yoo, H.; Polizzi, N. F.; Park, J.; Rawson, J.; Therien, M. J. *J. Am. Chem. Soc.* **2017**, *139*, 16946–16958.

(23) Ueno, K.; Misawa, H. *NPG Asia Mater.* **2013**, *5*, e61.

(24) Mack, J.; Kobayashi, N. *Chem. Rev.* **2011**, *111*, 281–321.

(25) Fukuda, T.; Homma, S.; Kobayashi, N. *Chem. Eur. J.* **2005**, *11*, 5205–5216.

(26) Zagal, J. H.; Griveau, S.; Silva, J. F.; Nyokong, T.; Bedioui, F. *Coord. Chem. Rev.* **2010**, *254*, 2755–2791.

(27) The conversion ratio was calculated from the absorption spectral changes at 1078

nm, which is attributed to the absorption of **1-H**$^{-\cdot}$. The molar absorption coefficient of **1-H**$^{-\cdot}$ was estimated from the absorption spectrum of **1-H**$^{-\cdot}$ generated by chemical reduction (Figure 4).

(28) Ratio of **1**$^{-}$ was estimated from the absorption spectral changes at 716 nm.

(29) Enomoto, T.; Kondo, M.; Asada, M.; Nakamura, T.; Masaoka, S. *J. Phys. Chem. C* **2018**, *122*, 11282–11287.

Chapter 3

In Situ Lipid Membrane Formation Triggered by an Intramolecular Photoinduced Electron Transfer

INTRODUCTION

Phospholipid membranes play a key role in defining the physical boundaries of living organisms.[1-2] A deeper understanding of membrane formation processes provides important insight into origin-of-life studies,[3-6] protein-membrane interactions,[7-9] drug-delivery systems,[10] and bottom-up synthetic biology.[11] One of the major goals of synthetic biology is the development of rational methodologies for the construction of self-assembling artificial membranes.[12] In living cells, phospholipid synthesis takes place by sequential enzymatic acyl transfer reactions of single-chain amphiphiles to a polar head group.[13-15] Recently, there has been significant interest in developing methodologies based on biomimetic coupling reactions capable of driving the de novo self-assembly of phospholipid membranes for creating artificial membrane systems.[16-18] However, spatiotemporal control of artificial phospholipid membrane formation is still a challenging objective.[17]

Given the interest in mimicking biological systems, we have recently developed a highly chemoselective methodology to promote phospholipid membrane formation by using copper-catalyzed azide-alkyne cycloaddition (CuAAC)[19-21] under mild aqueous conditions.[22] This approach employs a biomimetic coupling reaction to join an alkyl azide and an alkyne-modified lysophospholipid in presence of a copper(I) catalyst to produce an abiological triazole-containing phospholipid. After formation, the corresponding lipid product self-assembles to generate micron-sized membrane vesicles. Evidence from fluorescence microscopy suggests that cycloaddition reaction occurs at the interface of insoluble alkyl azide oil droplets and the monolayers of alkyne-modified lysophospholipid that coat the droplets. Devaraj and co-workers have previously utilized the CuAAC approach to design a self-reproducing catalyst that can drive the continual growth of phospholipid membranes.[23] More recently, they also demonstrated that the initiation of in situ vesicle formation can be stimulated photochemically.[24] Ruthenium(II)

tris(bipyridine) ($[Ru(bpy)_3]^{2+}$) complex was employed as a photoredox catalyst to convert resting copper(II) species to the active copper(I) catalyst via intermolecular photoinduced electron transfer (PET). Although intermolecular PET process is a powerful tool to manipulate the phospholipid membrane formation by photoirradiation,[24] the requirement of additives, photosensitizers and sacrificial electron donors makes the system complicated.[25] The author hypothesized that photoregulated vesicle formation could be dramatically simplified by using an intramolecular PET reaction. Because the PET reaction requires a single molecular species, no additives or sacrificial reductants would be necessary for the proposed system.

Here the author describes a new methodology of photoactivated in situ vesicle formation by triggering an intramolecular PET process using a copper-photosensitizer dyad (Figure 1). The author employed coumarin-3-carboxylic acid (CA) as a photosensitizer,[26-28] which is also capable of binding copper. Coumarin derivatives are well known to exhibit good photosensitizing properties,[26-28] but do not evoke phototoxic reactions.[29] In particular, CA acquires significant importance because it can coordinate to copper ions as a bidentate ligand via two carbonyl groups.[30] This fact makes possible the construction of efficient dyads for photoregulating relevant chemical reactions. Initially, the author demonstrated a CuAAC reaction mediated by a copper-coumarin dyad with water-soluble substrates and revealed that the reaction can be initiated by photoirradiation in the absence of any sacrificial reductants. Interestingly, the temporal control of CuAAC reaction is available by on/off switching of photoirradiation. The photocontrolled CuAAC reaction coupled to triazole phospholipid formation leads to a novel methodology for using light to initiate and control in situ vesicle formation.

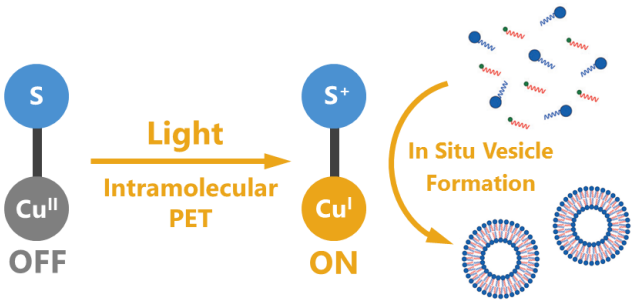

Figure 1. Schematic representation of in situ vesicle formation using a copper-sensitizer dyad [S = photosensitizer]. The intramolecular photoinduced electron transfer (PET) process is responsible for the generation of the active Cu(I) catalytic species, which subsequently triggers lipid synthesis and spontaneous vesicle formation.

RESULTS AND DISCUSSION

Photocontrolled CuAAC reaction of water-soluble substrates catalyzed by a copper-coumarin carboxylic acid dyad

The author initially demonstrated a CuAAC reaction using copper-CA dyad with water-soluble substrates, Boc-*L*-^{H}Ala(N_3)-OH·DCHA (**1**) and propalgylamine (**2**) (Scheme 1). Interestingly, the author found that temporal control of our CuAAC reaction is possible by on/off switching of photoirradiation. A reaction mixture containing **1**, **2**, Cu(II) salt, CA and TES buffer was illuminated by UV light (360 nm) (Figure 2) and then stored in the dark. The cycle was repeated, and the reaction was monitored at each switching point. The reaction time profile clearly shows distinct responses in triazole formation to light exposure, with the CuAAC reaction proceeding only under photoirradiation (Figure 3a). The author proposes that the temporal control is achieved via fast intramolecular back electron transfer (BET) process in copper-CA dyad (Figure 3b). Upon photoirradiation, copper-CA dyad is activated by intramolecular PET reaction, and CuAAC reaction proceeds. However, the activated copper-CA dyad is immediately deactivated through intramolecular BET reaction in the dark.[25] These forward and back electron transfer processes regulate the activation and deactivation pathway of the catalytic cycle.

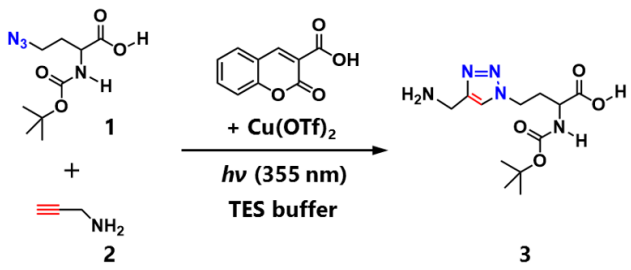

Scheme 1. Photocontrolled CuAAC reaction of water-soluble substrates catalyzed by copper-coumarin dyad. Precursors Boc-*L*-^{H}Ala(N_3)-OH·DCHA (**1**) and propargylamine (**2**) are efficiently coupled using a Cu(I) catalyst, which is generated in situ from a photoinduced electron transfer (PET) process on a Cu(II)-coumarin dyad.

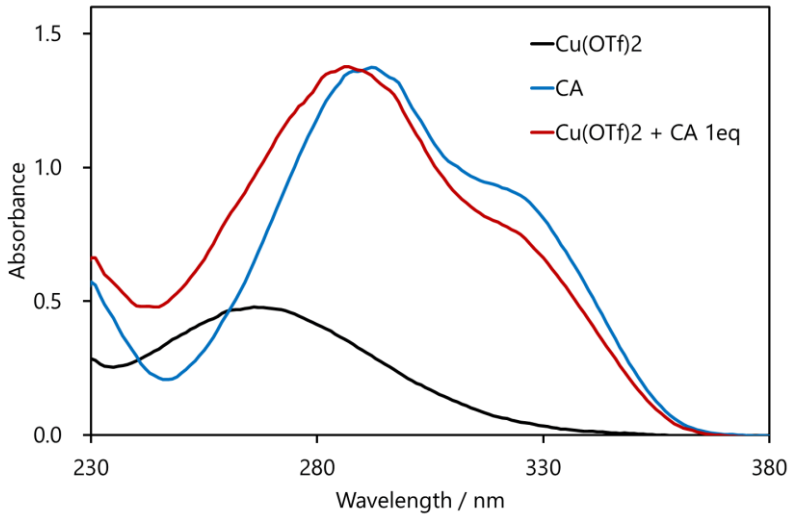

Figure 2. Absorption spectra of a 167 µM solution of $Cu(OTf)_2$ (*black*), a 167 µM solution of coumarin 3-carboxylic acid (CA) (*blue*) and an equimolar mixture (1:1; 167 µM final concentration of each) of $Cu(OTf)_2$ and CA (*red*).

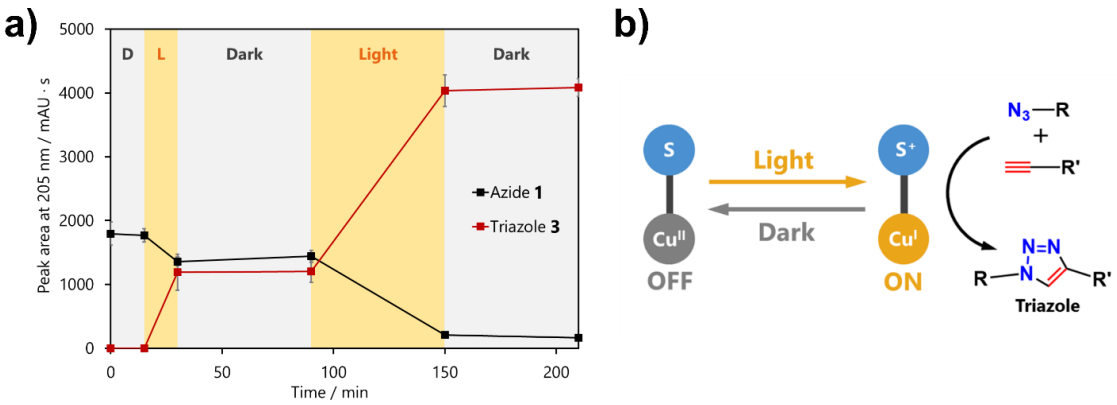

Figure 3. Triazole formation by photoinduced CuAAC reaction of water-soluble substrates. (a) Temporal control of the CuAAC reaction by on/off switching of photoirradiation. The consumption of the azide **1** and the formation of the corresponding triazole **3** was monitored over time by LC/MS [D: dark, L: light]. (b) Proposed mechanism for the photocontrolled CuAAC reaction of water-soluble substrates catalyzed by a copper-coumarin dyad [S = coumarin photosensitizer].

To verify the formation of the copper-CA dyad in reaction condition, fluorescence quenching experiments were carried out. Steady-state fluorescence measurements showed that CA has a characteristic emission band with a maximum at 413 nm upon excitation at 355 nm. The fluorescence emission was gradually quenched by addition of successive aliquots of a concentrated stock solution containing Cu(II) ions (Figure 4). From this result, we can infer that CA interacts with Cu(II) ions in these conditions, and the intramolecular PET process between CA and Cu(II) ion can proceed upon photoirradiation.

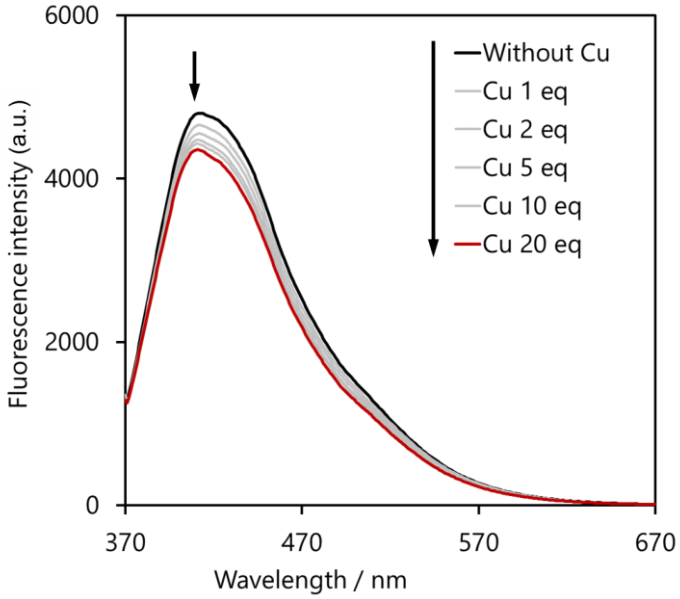

Figure 4. Fluorescence emission spectra of a 10 μM coumarin-3-carboxylic acid (CA) solution in 135 mM TES pH 8.5 buffer in the presence of $Cu(OTf)_2$ (from 0 to 20 equivalents) upon excitation at 355 nm. The solution also contains propalgylamine (**2**) (5 mM) and Boc-*L*-^{H}Ala(N_3)-OH·DCHA (**1**) (5 mM).

Photoinduced production of triazole phospholipid.

The author next applied the photoinduced CuAAC reaction for controlling in situ phospholipid membrane formation. We chose two appropriate substrates to mimic the native precursors of the common phospholipid 1-palmitoyl-2-oleoyl-sn-glycero-3-phosphocholine (POPC): an oleyl azide (**4**) in lieu of oleic acid and an alkyne analogue of the lysophospholipid 1-palmitoyl-sn-glycero-3-phosphocholine (**5**) (Scheme 2). Upon illuminating an aqueous dispersion of **5** containing **4**, Cu(II) salt and 1 equivalent of CA to Cu(II) ion in TES buffer (pH 8.5), precursors **4** and **5** were efficiently coupled to afford the corresponding triazole phospholipid **6** (Figure 5). No membranous structures could be found by phase contrast microscopy before photoirradiation (Figure 6). After continuous irradiation for 60 min, we observed the formation of both spherical and tubular vesicle structures on the periphery of the oleyl azide oil droplets (Figure 6). Lipid vesicular structures were also confirmed by fluorescence microscopy using the membrane-staining dyes Nile Red and/or Texas Red DHPE (Figure 7). These results illustrate that the photocontrolled CuAAC reaction using copper-CA dyad is capable to initiate biomimetic phospholipid membrane formation. Unfortunately, the temporal controllability of the CuAAC reaction was lost in these reaction conditions. The author also found that the phospholipid formation reaction did not terminate once the reaction was activated. The author hypothesizes that the heterogeneity of the reaction media inhibits the BET process of activated copper-CA dyad via hydrophobic interactions. After the intramolecular PET reaction of copper-CA dyad, the coumarin moiety can be dissociated as a neutral radical and extracted into the hydrophobic phase.[25,31] The charge separation process might inhibit the BET reaction to deactivate free Cu(I) catalyst to inactive Cu(II). Further studies will be necessary to describe a detailed mechanism for the intramolecular PET and BET processes, which could shed light on understanding the observed photocontrolled in situ vesicle formation phenomenon.

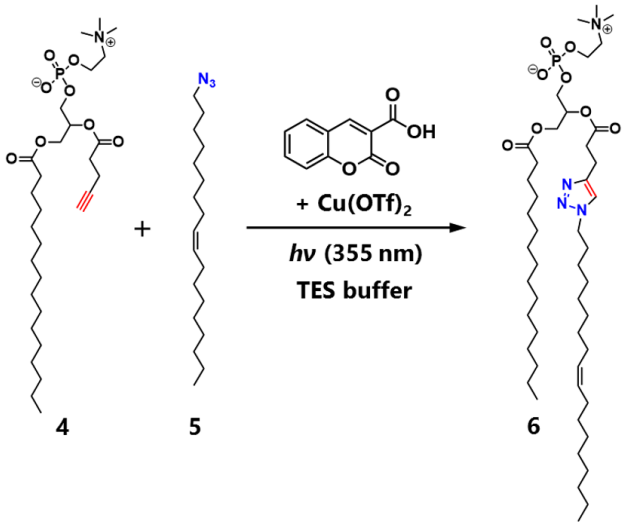

Scheme 2. Biomimetic synthesis of phospholipid membranes catalyzed by copper-coumarin dyad. Formation of triazole phospholipid **6** from the precursors alkyne lysophospholipid **4** and **5** is induced by a photocontrolled CuAAC reaction.

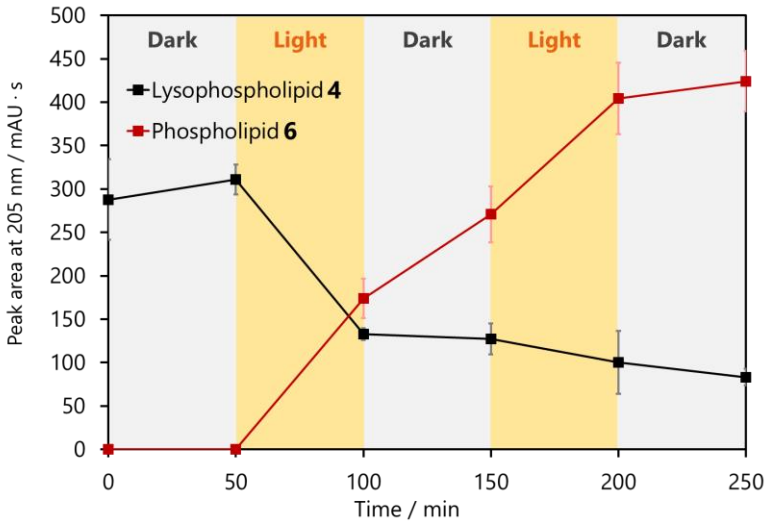

Figure 5. Reaction time profiles of phospholipid **6** formation with or without photoirradiation. The consumption of the alkyne lysophospholipid **4** and the formation of the corresponding triazole phospholipid **6** were monitored over time by LC/MS.

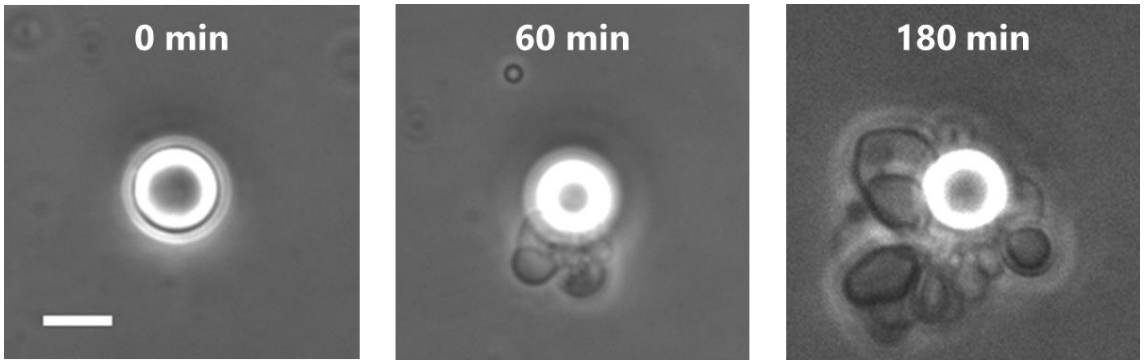

Figure 6. In situ vesicle formation driven by a photocontrolled bioorthogonal reaction. Phase-contrast microscopy images of the spontaneous assembly of phospholipid **6** into vesicular structures induced by a photocontrolled CuAAC reaction. Before photoirradiation (t = 0 min), phospholipid membranes were not present and only the emulsion oil droplets corresponding to the oleyl azide **5** were visible. However, the spontaneous formation of both tubular and spherical vesicular structures was observed over time upon light exposure. A large number of these membrane structures appeared at the periphery of the oleyl azide **5** droplets, suggesting that the CuAAC reactions occur at the interface of the insoluble droplets and the monolayers of alkyne lysolipid **4** that coat the droplets. Scale bar denotes 5 μm.

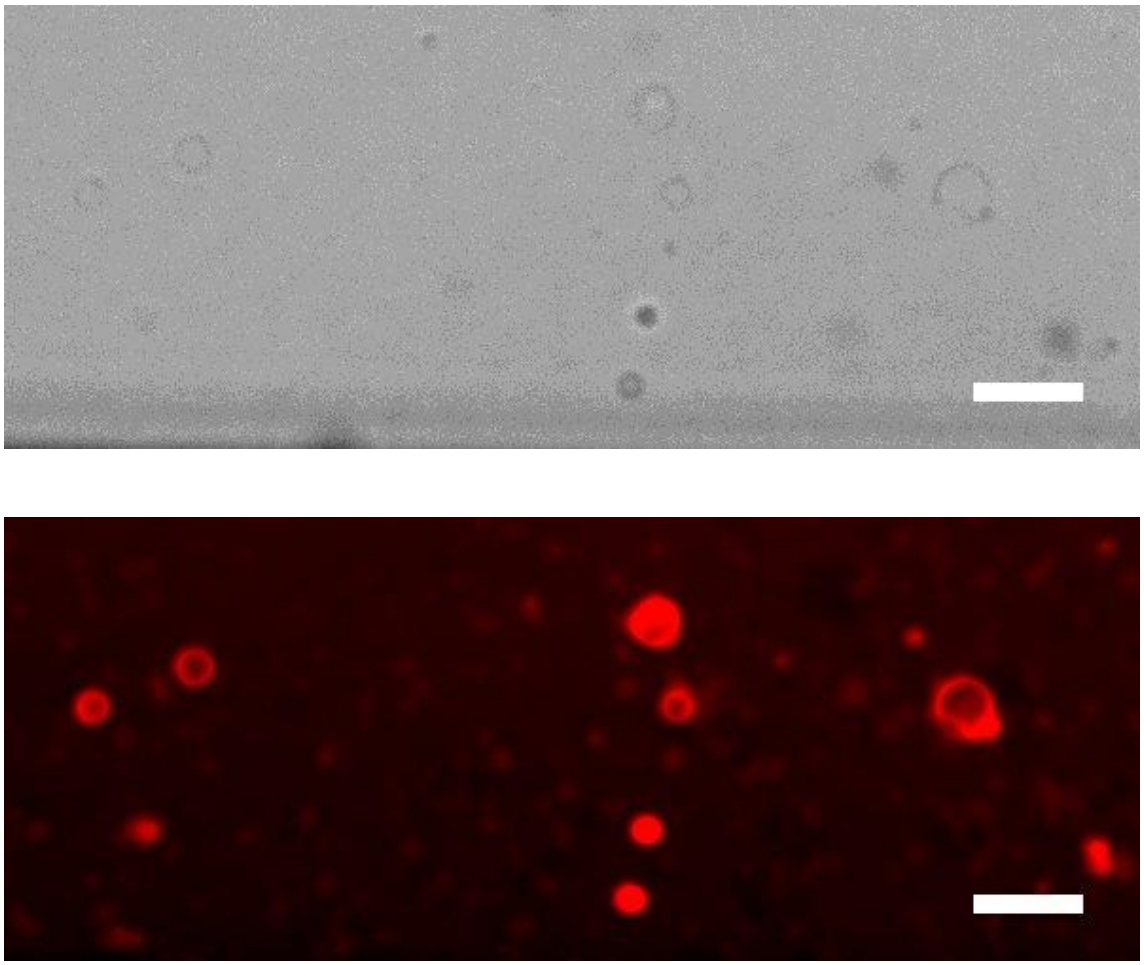

Figure 7. Spinning-disk confocal bright field (*top*) and fluorescence (*bottom*) microscope images of the membrane-containing vesicles formed by spontaneous assembly directed by a photocontrolled CuAAC-based synthesis of phospholipid **6**. Membranes were stained using 1 μM Nile Red dye solution. Scale bar denotes 5 μm.

CONCLUSION

We have developed a new methodology to promote biomimetic phospholipid membrane formation by photochemical activation of a CuAAC catalyst via an intramolecular PET process. The photochemical activation process proceeds without any sacrificial reductants. We also found that the copper-CA dyad works as a photocatalyst, controlling the CuAAC reaction by on/off switching of photoirradiation in homogeneous media. Our results offer future opportunities to exert spatiotemporal control over artificial cellular constructs.

EXPERIMENTAL SECTION

Chemicals and Materials

Commercially available 1-palmitoyl-2-hydroxy-*sn*-glycero-3-phosphocholine (Lyso C_{16} PC-OH) was used as purchased from Avanti® Polar Lipids. *N*-Boc-4-azido-*L*-homoalanine (dicyclohexylammonium salt) [Boc-*L*-^{H}Ala(N_3)-OH·DCHA, **1**], 4-pentynoic acid, 2,4,6-trichlorobenzoyl chloride (TCBC), triethylamine (Et_3N), 4-dimethylaminopyridine (DMAP), oleyl chloride, sodium azide, propargylamine (**2**), coumarin-3-carboxylic acid (CA), copper(II) triflluoromethanesulfonate [copper(II) triflate; $Cu(OTf)_2$] and *N*-[tris(hydroxylmethyl)methyl]-2-aminoethanesulfonic acid (TES), sodium salt were obtained from Sigma-Aldrich. Nile Red and Texas Red® 1,2-dihexadecanoyl-*sn*-glycero-3-phosphoethanolamine, triethylammonium salt (Texas Red® DHPE) were obtained from Life Technologies. Deuterated chloroform ($CDCl_3$) was obtained from Cambridge Isotope Laboratories. All reagents obtained from commercial suppliers were used without further purification unless otherwise noted. Analytical thin-layer chromatography was performed on E. Merck silica gel 60 F_{254} plates. Compounds, which were not UV active, were visualized by dipping the plates in a potassium permanganate solution and heating. Silica gel flash chromatography was performed using E. Merck silica gel (type 60SDS, 230-400 mesh). Solvent mixtures for chromatography are reported as v/v ratios. HPLC analysis was carried out on an Eclipse Plus C8 analytical column with *Phase A*/*Phase B* gradients [*Phase A*: H_2O with 0.1% formic acid; *Phase B*: MeOH with 0.1% formic acid]. HPLC purification was carried out on Zorbax SB-C18 semipreparative column with *Phase A*/*Phase B* gradients [*Phase A*: H_2O with 0.1% formic acid; *Phase B*: MeOH with 0.1% formic acid]. Proton nuclear magnetic resonance (^{1}H NMR) spectra were recorded on a Varian VX-500 MHz spectrometer, and were referenced relative to residual proton resonances in $CDCl_3$ (at 7.24 ppm). Chemical shifts were reported in parts per million (ppm, δ) relative to tetramethylsilane (δ 0.00). ^{1}H NMR splitting patterns are assigned as singlet (s), doublet (d), triplet (t), quartet (q) or pentuplet (p). All first-order splitting patterns were designated on the basis of the appearance of the multiplet. Splitting patterns that could not be readily interpreted are designated as multiplet (m) or broad (br). Carbon nuclear magnetic resonance (^{13}C NMR) spectra were

recorded on a Varian VX-500 MHz spectrometer, and were referenced relative to residual proton resonances in $CDCl_3$ (at 77.23 ppm). Electrospray Ionization-Time of Flight (ESI-TOF) spectra were obtained on an Agilent 6230 Accurate-Mass TOFMS mass spectrometer. UV/Vis measurements were made on a NanoDrop 2000C spectrophotometer (Thermo Fisher Scientific, USA), using UV/Vis quartz cuvettes and/or Cary UV disposable cells (polystyrene, rectangular micro cells; path length: 10 mm, sample chamber width: 4 mm). Fluorescence measurements were obtained on a JASCO FP-8500 spectrofluorometer, using fluorescence quartz cuvettes. All photoreactions were performed on a Rayonet photochemical reactor (The Southern New England Ultraviolet Co., USA) equipped with UV lamps (360 nm). Wilmad® quartz (CFQ) EPR tubes (O.D.: 5 mm, L: 100 mm) were obtained from Sigma-Aldrich. Microscopy images were acquired on a BX51 optical microscope (Olympus, Japan), using bright-field/phase-contrast illumination with a 100x, 1.30 NA oil immersion objective. Spinning-disk confocal microscopy images were acquired on a Yokagawa spinning disk system (Yokagawa, Japan) built around an Axio Observer Z1motorized inverted microscope (Carl Zeiss Microscopy GmbH, Germany) with a 63x, 1.40 NA oil immersion objective to an Evolve 512x512 EMCCD camera (Photometrics, Canada) using ZEN imaging software (Carl Zeiss Microscopy GmbH, Germany). A condenser/objective with a phase stop of Ph2 was used to obtain the phase-contrast images. The fluorophore (Nile Red and/or Texas Red®) was excited with a 561 nm, 40 mW DPSS laser.

Synthesis of phospholipid precursors

*3-(Palmitoyloxy)-2-(pent-4-ynoyloxy)propyl[2-(trimethylammonio)ethyl] phosphate (Alkyne lysophospholipid, **4**).*[22] A solution of 1-palmitoyl-2-hydroxy-*sn*-glycero-3-phosphocholine (**Lyso C_{16} PC-OH**, 47.5 mg, 95.8 μmol), 4-pentynoic acid (23.5 mg, 239.5 μmol), DMAP (70.2 mg, 574.8 μmol) and Et_3N (46.7 μL, 335.3 μmol) in $CDCl_3$ (3.75 mL) was stirred at r.t. for 10 min. Then, TCBC (97.3 μL, 622.7 μmol) was added. After 12 h stirring at r.t., H_2O (250 μL) was added to quench the acid chloride, and the solvent was removed under reduced pressure to give a pale yellow solid. The corresponding residue was dissolved in MeOH (1 mL), filtered using a 0.2 μm syringe-driven filter, and the crude solution was purified by HPLC, affording 47.1 mg of **4** as a

white solid [85%, t_R = 11.6 min (Zorbax SB-C18 semipreparative column, 50% *Phase A* in *Phase B*, 5 min, and then 5% *Phase A* in *Phase B*, 10 min)]. ^{1}H NMR ($CDCl_3$, 500.13 MHz, δ): 5.31-5.16 (m, 1H, 1 × CH), 4.43-4.23 (m, 3H, 1.5 × CH_2), 4.22-4.07 (m, 1H, 0.5 × CH_2), 4.06-3.92 (m, 2H, 1 × CH_2), 3.87-3.70 (m, 2H, 1 × CH_2), 3.32 (s, 9H, 3 × CH_3), 2.64-2.52 (m, 2H, 1 × CH_2), 2.51-2.41 (m, 2H, 1 × CH_2), 2.28 (t, *J* = 7.7 Hz, 2H, 1 × CH_2), 2.09 (t, *J* = 2.5 Hz, 1H, 1 × CH), 1.69-1.45 (m, 2H, 1 × CH_2), 1.38-1.10 (m, 24H, 12 × CH_2), 0.87 (t, *J* = 7.0 Hz, 3H, 1 × CH_3). ^{13}C NMR ($CDCl_3$, 125.77 MHz, δ): 173.7, 171.5, 82.6, 71.2, 69.7, 66.4, 63.7, 62.7, 59.5, 54.6, 34.2, 33.4, 32.1, 29.9, 29.8, 29.8, 29.7, 29.5, 29.5, 29.3, 25.0, 22.8, 14.3. MS (ESI-TOF) [m/z (%)]: 598 ([M +Na]$^+$, 68), 576 ([MH]$^+$, 100). HRMS (ESI-TOF) calculated for $C_{29}H_{54}NO_8PNa$ ([M +Na]$^+$) 598.3479, found 598.3482.

(Z)-1-Azidooctadec-9-ene (Oleyl azide, ***5****).*[22] To a solution of oleyl chloride (126.1 mg, 0.44 mmol) in DMF (1 mL) was added sodium azide (100.0 mg, 1.54 mmol), and the resulting mixture was heated at 85 ºC under argon for 12 h. Afterward, H_2O (5 mL) was added, and the desired oleyl derivative was extracted with CH_2Cl_2 (3×10 mL). The combined organic layers were dried (Na_2SO_4), filtered and concentrated, providing a yellow oil, which was purified by flash chromatography (0-1% EtOAc in hexane), affording 105.3 mg of **5** as a pale yellow oil [82%, R_f = 0.50 (1% EtOAc in hexane)]. ^{1}H NMR ($CDCl_3$, 500.13 MHz, δ): 5.48-5.19 (m, 2H, 2 × CH), 3.25 (t, *J* = 7.0 Hz, 2H, 1 × CH_2), 2.14-1.87 (m, 4H, 2 × CH_2), 1.71-1.51 (m, 2H, 1 × CH_2), 1.47-1.15 (m, 22H, 11 × CH_2), 0.88 (t, *J* = 7.0 Hz, 3H, 1 × CH_3). ^{13}C NMR ($CDCl_3$, 125.77 MHz, δ): 130.1, 129.9, 51.6, 32.1, 29.9, 29.9, 29.7, 29.5, 29.5, 29.5, 29.3, 29.3, 29.0, 27.4, 27.3, 26.9, 22.9, 14.3. MS (ESI-TOF) [m/z (%)]: 294 ([MH]$^+$, 15). HRMS (ESI-TOF) calculated for $C_{18}H_{36}N_3$ ([MH]$^+$) 294.2909, found 294.2938.

Photocontrolled CuAAC reaction of water-soluble substrates

245 μL of 135 mM TES pH 8.5 buffer, 15 μL of a 100 mM solution of propalgylamine (**2**) in 135 mM TES pH 8.5 buffer, 30 μL of a 50 mM solution of Boc-*L*-^{H}Ala(N_3)-OH·DCHA (**1**) in 135 mM TES pH 8.5 buffer, 5 μL of a 15 mM solution of CA in 135 mM TES pH 8.5 buffer, and 5 μL of a 15 mM solution of $Cu(OTf)_2$ in 135 mM TES pH 8.5 buffer were added to a Wilmad® quartz (CFQ) EPR tube (O.D.: 5 mm, L: 100 mm).

The solution was degassed by Ar bubbling for 30 min and irradiated with UV light (360 nm) on a photochemical reactor at room temperature. The reaction was monitored over time by HPLC/MS analysis, observing the formation of the triazole **3**.

Fluorescence quenching of coumarin sensitizer by copper ion

A 10 μM solution of CA in 135 mM TES pH 8.5 buffer containing 5 mM of propalgylamine (**2**) and 5 mM of Boc-*L*-^{H}Ala(N_3)-OH·DCHA (**1**) was excited at 355 nm, and the fluorescence spectra were recorded on a spectrofluorometer between 370 and 700 nm. Then, the author performed serial additions of a 1.5 mM solution of $Cu(OTf)_2$ in 135 mM TES pH 8.5 buffer to the coumarin solution (from 0 to 20 equivalents of $Cu(OTf)_2$ respect to CA). The corresponding fluorescence spectral changes were monitored on a spectrofluorometer.

In situ vesicle formation regulated by photocontrolled CuAAC reaction

50 μL of a 10 mM solution of oleyl azide (**5**) in MeOH was added to a Wilmad® quartz (CFQ) EPR tube (O.D.: 5 mm, L: 100 mm) and dried under reduced pressure. Then, 140 μL of 135 mM TES pH 8.5 buffer, 50 μL of a 10 mM solution of the alkyne lysophospholipid (**4**) in 135 mM TES pH 8.5 buffer, 5 μL of a 10 mM solution of CA in 135 mM TES pH 8.5 buffer, and 5 μL of a 10 mM solution of $Cu(OTf)_2$ in 135 mM TES pH 8.5 buffer were successively added. The resulting solution was sonicated 5 min and subsequently vortexed 1 min to obtain a cloudy emulsion. The resulting emulsion was degassed by repetitive freeze-thaw cycles (3 times) and irradiated with UV light (360 nm) on a photochemical reactor at room temperature. The reaction was monitored over time by HPLC/MS analysis (observing the formation of the triazole phospholipid **6**) and microscopy imaging (observing the spontaneous phospholipid **6** vesicle generation).

HPLC/ELSD/MS Analysis

De novo formation of phospholipid membranes was performed in the appropriate buffer (135 mM TES pH 8.5 buffer) as described above. Aliquots of 10 μL of sample were taken at various time points and analyzed using an Eclipse Plus C8 analytical column (5%

Phase A in *Phase B*, 5.5 min) with an Evaporative Light Scattering Detector (ELSD) at a flow of 1.0 mL/min. For all HPLC/MS runs, solvent *Phase A* consisted of H_2O with 0.1% formic acid and solvent *Phase B* of MeOH with 0.1% formic acid.

REFERENCES

(1) Jesorka, A.; Orwar, O. *Annu. Rev. Anal. Chem.* **2008**, *1*, 801-832.

(2) van Meer, G.; Voelker, D. R.; Feigenson, G. W. *Nat. Rev. Mol. Cell Biol.* **2008**, *9*, 112-124.

(3) Deamer, D. W. *Microbiol. Mol. Biol. Rev.* **1997**, *61*, 239-261.

(4) Luisi, P. L.; Walde, P.; Oberholzer, T. *Curr. Opin. Colloid In.* **1999**, *4*, 33-39.

(5) Hanczyc, M. M.; Fujikawa, S. M.; Szostak, J. W. *Science* **2003**, *302*, 618-622.

(6) Kurihara, K.; Okura, Y.; Matsuo, M.; Toyota, T.; Suzuki, K.; Sugawara, T. *Nat. Commun.* **2015**, *6*, 8352.

(7) Di Paolo, G.; De Camilli, P. *Nature* **2006**, *443*, 651-657.

(8) Zhao, H.; Lappalainen, P. *Mol. Biol. Cell.* **2012**, *23*, 2823-2830.

(9) Saliba, A.-E.; Vonkova, I.; Ceschia, S.; Findlay, G. M.; Maeda, K.; Tischer, C.; Deghou, S.; van Noort, V.; Bork, P.; Pawson, T.; Ellenberg, J.; Gavin, A. C. *Nat. Methods* **2014**, *11*, 47-50.

(10) Kraft, J. C.; Freeling, J. P.; Wang, Z.; Ho, R. J. *J. Pharm. Sci.* **2014**, *103*, 29-52.

(11) Rivas, G.; Vogel, S. K.; Schwille, P. *Curr. Opin. Chem. Biol.* **2014**, *22C*, 18-26.

(12) Brea, R. J.; Hardy, M. D.; Devaraj, N. K. *Chem. Eur. J.* **2015**, *21*, 12564-12570.

(13) Zhang, Y. M.; Rock, C. O. *J. Lipid Res.* **2008**, *49*, 1867-1874.

(14) Shindou, H.; Hishikawa, D.; Harayama, T.; Yuki, K.; Shimizu, T. *J. Lipid Res.* **2009**, *50 Suppl.*, S46-S51.

(15) Holthuis, J. C.; Menon, A. K. *Nature* **2014**, *510*, 48-57.

(16) Brea, R. J.; Cole, C. M.; Devaraj, N. K. *Angew. Chem. Int. Ed.* **2014**, *53*, 14102-

14105.

(17) Konetski, D.; Gong, T.; Bowman, C. N. *Langmuir* **2016**, *32*, 8195-8201.

(18) Devaraj, N. K. *J. Org. Chem.* **2017**, *82*, 5997-6005.

(19) Meldal, M.; Tornoe, C. W. *Chem. Rev.* **2008**, *108*, 2952-3015.

(20) Tornoe, C. W.; Christensen, C.; Meldal, M. *J. Org. Chem.* **2002**, *67*, 3057-3064.

(21) Rostovtsev, V. V.; Green, L. G.; Fokin, V. V.; Sharpless, K. B. *Angew. Chem. Int. Ed.* **2002**, *41*, 2596-2599.

(22) Budin, I.; Devaraj, N. K. *J. Am. Chem. Soc.* **2012**, *134*, 751-753.

(23) Hardy, M. D.; Yang, J.; Selimkhanov, J.; Cole, C. M.; Tsimring, L. S.; Devaraj, N. K. *Proc. Natl. Acad. Sci. U.S.A.* **2015**, *112*, 8187-8192.

(24) Hardy, M. D.; Konetski, D.; Bowman, C. N.; Devaraj, N. K. *Org. Biomol. Chem.* **2016**, *14*, 5555-5558.

(25) El-Khouly, M. E.; Ito, O.; Smith, P. M.; D'Souza, F *J. Photoch. Photobio. C* **2004**, *5*, 79-104.

(26) Specht, D. P.; Martic, P. A.; Farid, S. *Tetrahedron* **1982**, *38*, 1203-1211.

(27) Williams, J. L. R.; Specht, D. P.; Farid, S. *Polym. Eng. Sci.* **1983**, *23*, 1022-1024.

(28) Kuznetsova, N. A.; Kaliya, O. L. *Russ. Chem. Rev.* **1992**, *61*, 1243-1267.

(29) Kaidbey, K. H.; Kligman, A. M. *Arch. Dermatol.* **1981**, *117*, 258-263.

(30) Cui, Y.; Gao, Q.; Wang, H. H.; Wang, L.; Xie, Y. B *Acta Crystallogr. E* **2011**, *67*, m782.

(31) Limburg, B.; Laisne, G.; Bouwman, E.; Bonnet, S. *Chem. Eur. J.* **2014**, *20*, 8965-8972.

Concluding Remarks

The research described in this thesis has been carried out from three points of view for further development of PET; an extension of usable energy of photons in PET reaction to the longer wavelength region than visible light, a conjugation of PET reaction with other chemical reactions, and an application of PET for controlling chemical reaction. The author established three novel photochemical systems based on PET in this thesis.

Chapter 1 describes the first example of NIR-ET system via dynamic quenching mechanism. The key to the success is an employment of a distorted phthalocyanine derivative with appropriate modification, which shows high photostability and long excitation lifetime. The discovery offers future opportunities to the development of new class of PET systems driven by NIR light.

Chapter 2 shows a PCET system driven by NIR light for the first time. A phthalocyanine anion which exhibits intense NIR absorption property and electron transfer and proton accepting abilities promoted a PCET reaction induced by NIR light (> 710 nm). The NIR light induced PCET system can generate long-lived radical species by suppressing a back electron transfer reaction and showed high reversibility and robustness. The result will pave the way for developing photoinduced PCET systems driven by NIR light.

Chapter 3 describes a new methodology to promote a biomimetic phospholipid membrane formation by a photochemical activation of a catalyst-sensitizer dyad using an intramolecular PET process. The photocontrolled CuAAC reaction coupled to triazole phospholipid formation leads to a novel methodology for using light to initiate the vesicle formation.

The results shown in this thesis provide both fundamental insights (Chapter 1 and 2) and a new application (Chapter 3) of PET. These studies may contribute to the growth of the research field of PET.

List of Publications

Chapter 1

"Near-IR Light-Induced Electron Transfer via Dynamic Quenching"

Takafumi Enomoto, Mio Kondo, Mizue Asada, Toshikazu Nakamura, and Shigeyuki Masaoka
J. Phys. Chem. C, **2018**, *122*, 11282–11287.

Chapter 2

"Proton-Coupled Electron Transfer Induced by Near-Infrared Light"

Takafumi Enomoto, Mio Kondo, and Shigeyuki Masaoka
Manuscript in preparation.

Chapter 3

"In Situ Lipid Membrane Formation Triggered by an Intramolecular Photoinduced Electron Transfer"

Takafumi Enomoto, Roberto J. Brea, Ahanjit Bhattacharya, and Neal K. Devaraj
Langmuir, **2018**, *34*, 750–755.

Other Publications

"Titania may produce abiotic oxygen atmospheres on habitable exoplanets"

Norio Narita, **Takafumi Enomoto**, Shigeyuki Masaoka, and Nobuhiko Kusakabe
Sci. Rep., **2015**, *5*, 13977.

"C(sp3)-H Cyanation Promoted by Visible-Light Photoredox/Phosphate Hybrid Catalysis"

Takayuki Wakaki, Kentaro Sakai, **Takafumi Enomoto**, Mio Kondo, Shigeyuki Masaoka, Kounosuke Oisaki, and Motomu Kanai
Chem. Eur. J., **2018**, *24*, 8051–8055.

"Function-integrated Ru catalyst for photochemical CO2 reduction"

Sze Koon Lee, Mio Kondo, Masaya Okamura, **Takafumi Enomoto**, Go Nakamura, and Shigeyuki Masaoka
J. Am. Chem. Soc., **2018**, *140*, 16899–16903.